Published in final edited form as:
Methods. 2009 October ; 49(2): 148–166. doi:10.1016/j.ymeth.2009.07.005.

IDENTIFICATION OF CATALYTIC METAL ION LIGANDS IN RIBOZYMES

John K. Frederiksen[a] and **Joseph A. Piccirilli**[b,c,d,*]

[a]The Pritzker School of Medicine, The University of Chicago, 929 East 57th Street, Chicago, Illinois 60637

[b]Department of Biochemistry and Molecular Biology, The University of Chicago, 929 East 57th Street, Chicago, Illinois 60637

[c]Department of Chemistry, The University of Chicago, 929 East 57th Street, Chicago, Illinois 60637

[d]Howard Hughes Medical Institute, The University of Chicago, 929 East 57th Street, Chicago, Illinois 60637

Abstract

Site-bound metal ions participate in the catalytic mechanisms of many ribozymes. Understanding these mechanisms therefore requires knowledge of the specific ligands on both substrate and ribozyme that coordinate these catalytic metal ions. A number of different structural and biochemical strategies have been developed and refined for identifying metal ion binding sites within ribozymes, and for assessing the catalytic contributions of the metal ions bound at those sites. We review these approaches and provide examples of their application, focusing in particular on metal ion rescue experiments and their roles in the construction of the transition state models for the *Tetrahymena* group I and RNase P ribozymes.

Introduction: Metal ions and RNA catalysis

The ability of ribozymes to perform catalysis depends critically on metal ions. Their impact on catalysis is threefold. On the one hand, they screen the negative charges of the phosphodiester backbone, allowing ribozymes to fold into their active three-dimensional structures. Metal ions also coordinate functional groups on both substrates and ribozymes to position reactants and stabilize developing transition states. In addition, hydrated metal ions may donate or accept protons to facilitate general acid-base catalysis. In these ways, metal ions help ribozymes to achieve rate accelerations of as much as 10^{11}-fold (1).

A complete understanding of the mechanisms underlying ribozyme catalysis requires a detailed description of where metal ions bind within the catalytic site. This includes the identification of specific ligands on both substrate and ribozyme that coordinate the catalytic metal ions, enabling the construction of models of the transiently-formed transition state. RNA provides a number of different ligands that can potentially bind metal ions, including

*To whom correspondence should be addressed. Phone: (773) 702-9312, Fax: (773) 702-0271, jpicciri@uchicago.edu.

both bridging and nonbridging phosphate oxygens, ribose 2'-OH groups, and nucleobase functional groups (purine N7 and O6, for example). The diffuse ion atmosphere that surrounds RNA makes the isolation of any single metal ion-ligand interaction a formidable challenge. Nevertheless, a number of experimental strategies have been developed that make possible the assignment of specific atoms as ligands for catalytic metal ions within ribozymes (Figure 1). This paper will describe several of these techniques, from the detection of metal ion binding sites to experiments that link metal ions to individual atoms in the transition state.

Enzymologic considerations

Identifying ligands that bind the catalytic metal ions within a given ribozyme should include a thorough exploration of ribozyme enzymology. This includes determining the dependence of the reaction rate on substrate and enzyme concentrations, monovalent and divalent metal ion concentrations, ionic strength, and pH, among other variables. Equilibrium and kinetic binding parameters of substrates, cofactors, and products should be obtained with the goal of producing a rigorous description of the pathways taken from reactants to products. Although the kinetic model for a ribozyme reaction does not identify catalytic metal ion ligands *per se*, it does provide the experimental framework within which a meaningful ligand search can occur.

An especially important consideration is the dependence of the reaction rate on metal ion concentration. Initially, ribozymes were thought to be absolutely dependent on divalent metal ions for catalysis (2). This is true for the so-called "large" ribozymes that catalyze the attack of an external nucleophile on phosphorous (the group I and group II introns, RNase P, and the spliceosome). However, the discovery that high concentrations of monovalent ions support catalysis by the endonucleolytic ribozymes (the hammerhead, hairpin, VS, HDV, and *glmS* ribozymes) (3–6) has prompted a reexamination of how metal ions function in ribozyme catalysis (7). "Catalytic" roles for metal ions now include stabilization of active tertiary structures through nonspecific electrostatic effects, participation in general acid-base catalysis, modification of functional group pK_a values, and site binding. A careful analysis of the mono- and divalent metal ion dependences of the reaction can help to distinguish among these possibilities. One strategy has been to monitor the divalent metal ion concentration dependence of the reaction in a background of elevated monovalent metal ion concentration (usually in the molar range). The high concentration of monovalent metal ions excludes divalent metal ions from the diffuse ion atmosphere (8). Site-bound divalent metal ions may then be characterized with respect to a number of different quantitative parameters, including binding affinity, the pH dependence of binding, and the ability of other ions to compete for different sites.

Using this approach, Bevilacqua and colleagues have performed an extensive analysis of the Mg^{2+}- and pH-dependences of the reaction catalyzed by the hepatitis delta virus (HDV) ribozyme. Their experiments have led to a model (Figure 2) in which the ribozyme reacts via one of three separate channels depending on the concentration of Mg^{2+} ions (9). In the absence of Mg^{2+}, the ribozyme reacts at a basal rate dependent only on the presence of 1 M NaCl (Figure 2, channel 1). Low concentrations of Mg^{2+} (10^{-9} to 10^{-7} M) do not affect this rate significantly. In contrast, intermediate concentrations of Mg^{2+} (10^{-7} to 10^{-4} M) accelerate the reaction rate in a log-linear fashion, consistent with a change in the predominant reaction pathway (Figure 2, channel 2). At higher Mg^{2+} concentrations (10^{-4} to 10^{-1} M), the reaction rate becomes independent of Mg^{2+} concentration, signifying a third pathway for product formation (Figure 2, channel 3).

Under channel 1 conditions, the reaction rate increases log-linearly with pH up to about 6, and decreases thereafter. This pH-rate profile persists at intermediate Mg^{2+} concentrations (channel 2). However, at high Mg^{2+} concentrations (channel 3) the reaction rate becomes independent of pH above 6. These distinct pH-rate profiles for channels 2 and 3 prompted the hypothesis that two different classes of Mg^{2+} ions accelerate the reaction rate of the HDV ribozyme. One Mg^{2+} ion facilitates catalysis by binding to a structural metal ion site at intermediate Mg^{2+} concentrations (channel 2). This interaction is thought to occur through inner sphere coordination, since the affinity decreases with increasing ionic radius and is not affected by the presence of the exchange-inert metal complex $Co(NH_3)_6^{3+}$ (10). In addition, the binding of the structural metal ion decreases with increasing pH (9), suggesting that binding may be linked to a protonation event. In fact, subsequent work has provided evidence that this structural metal ion binds tightly to a base quadruple whose stability depends critically on the protonation state of C41 (11).

At high Mg^{2+} concentrations (channel 3), a second ion contributes to catalysis. As the rate for channel 3 is independent of pH above 6, this ion must offset the inhibitory titration that occurs above pH 6 for channels 1 and 2. Consequently, the ion is thought to play a catalytic, rather than a purely structural, role in HDV ribozyme catalysis. In contrast to the structural ion, the binding affinity of the catalytic ion does not correlate with ionic radius, and $Co(NH_3)_6^{3+}$ inhibits the channel 3 reaction pathway (10). These observations suggest that the catalytic metal ion binds to its site via outer sphere coordination. The ion binds more tightly to its site as the pH increases (9), consistent with its proposed role as a general base in the HDV ribozyme reaction. Subsequent crystallographic (12) and spectroscopic (13) work has provided additional evidence for the existence and function of this catalytic metal ion.

X-ray crystallography

Crystal structures of ribozymes have provided a wealth of information about the local and global architectures underlying the mechanisms of catalysis. Crystals that diffract to sufficient resolution can reveal the positions, coordination geometries, and local environments of metal ions (usually Mg^{2+} and K^+), suggesting possible ligands for further investigation. For lower resolution structures, soaking the crystals in heavier metals such as Tl^+, Mn^{2+}, Pb^{2+}, Co^{3+}, Os^{3+}, Eu^{3+}, or Ir^{3+} can aid in identifying metal ion binding sites and assist in phasing. This can be especially helpful in distinguishing Mg^{2+} ions from water molecules and other ionic species, which may yield similar patterns of electron density (14). Crystal structures of nearly all of the naturally occurring ribozymes have been solved, including the group I (15–18) and group II (19, 20) introns, RNase P (21–23), the ribosome (24–26), and the hammerhead (27–31), hairpin (32, 33), HDV (12, 34, 35), and *glmS* (36) ribozymes. In addition, RNA-binding proteins have improved our ability to crystallize RNA (12, 15, 32, 35, 37), whose negatively-charged backbone and relative lack of crystal contacts have been thought to impede the formation of well-ordered crystals (35). Despite their atomic-level detail, crystal structures of ribozymes have limitations with respect to their ability to predict whether apparent contacts between metal ions and ligands are relevant to the catalytic mechanism. By definition, a crystal structure is a model of a *ground state* conformation of the ribozyme, and not necessarily the most highly populated conformation in solution. This model may show metal ions and ribozyme functional groups in a configuration consistent with a proposed catalytic mechanism. However, the model does not prove that this mechanism actually occurs, or that the atoms involved function in the manner suggested by their arrangement. Moreover, different crystal structures of the same molecule may include different numbers of metal ions within the catalytic site. Structures of the same restriction endonuclease, for example, may show zero, one, two, or even three possible catalytic metal ions (38–40). Furthermore, crystal structures are snapshots of molecules in

an instant of time under specific ionic conditions, and may not reflect the local or global dynamics that can contribute to catalysis. Instead, crystal structures are most effective at elucidating mechanism when they are interpreted in conjunction with experiments that test the functionality of the proposed catalytic players. The discrepancies between the biochemical behavior of the minimal hammerhead ribozyme and the models derived from hammerhead crystal structures (41) underscore the need to correlate both structural and functional data when investigating mechanism.

Spectroscopic methods

Several different spectroscopies have been used to locate and characterize metal ion binding sites within ribozymes. These techniques are sensitive to the coordination environment surrounding a given metal ion, and hence are especially effective at defining metal ion ligands and monitoring changes in coordination over time.

Electron paramagnetic resonance and nuclear magnetic resonance methods have found many applications in the study of interactions between metal ions and RNA. Electron paramagnetic resonance (EPR) experiments monitor signals from the spins of unpaired electrons, which may be present in either organic radicals or paramagnetic metal ions (42). As applied to metal ion binding sites in RNA, EPR relies on the ability of the paramagnetic Mn^{2+} ion ($S = 5/2$) to substitute functionally for Mg^{2+}, which is diamagnetic. Mn^{2+} produces a distinctive six-peak EPR pattern that changes subtly, yet reproducibly, with RNA-induced alterations in the ion's coordination sphere (Figure 3A). Monitoring these changes as a function of Mn^{2+} concentration yields binding association constants and cooperativities, as well as the number of different classes of ions that bind the RNA. Ligand identity may be inferred by using higher resolution EPR techniques such as ENDOR (electron nuclear double resonance) and ESEEM (electron spin echo envelope modulation), which report on the interactions between the unpaired Mn^{2+} electron and surrounding nuclei. These methods have helped to characterize a high-affinity Mn^{2+} binding site ($K_d \leq 10$ μM in 1 M NaCl) within the minimal and full-length hammerhead ribozymes (43–46) (Figure 3B).

In addition to its use in RNA structure determination (47–52), nuclear magnetic resonance (NMR) is also a sensitive reporter of metal ion-induced changes in secondary and tertiary structure. Metal ion binding alters the chemical shifts of NMR-active nuclei within RNA. Provided that these chemical shifts can be assigned reliably, NMR can monitor conformational changes associated with metal binding, as well as the geometries of the binding sites. Mg^{2+}-induced conformational rearrangements have been demonstrated for a number of RNAs, including the P5abc domain from the group I ribozyme (53) and the transactivation response element (TAR) RNA from HIV-1 (54). Site-specific incorporation of phosphorothioates or spin-labeled nuclei (^{2}H, ^{13}C, ^{15}N) can simplify the interpretation of NMR spectra and provide additional distance constraints within RNAs. For example, NMR was used to follow Cd^{2+} binding to phosphorothioate substitutions within the aforementioned high-affinity metal ion site in the hammerhead ribozyme (55). Subsequently, a combined NMR and EPR approach in the context of $^{2}H_2O$ and ^{15}N-labeled guanine helped to define the coordination environment of a Mn^{2+} ion bound at this site (46). The paramagnetic Mn^{2+} ion has also found applications in pure NMR experiments that exploit the ability of bound Mn^{2+} ions to broaden the NMR signals from nearby ligands. This strategy helped to identify metal ion binding sites within the hairpin ribozyme (56) and an adenine-sensing riboswitch (57). In addition, direct measurements of metal ion binding are possible with NMR-active nuclei such as ^{25}Mg (58, 59), ^{59}Co (60), ^{23}Na (61–63), and ^{105}Tl (64).

Other spectroscopic methods used to study metal ion-RNA interactions include X-ray absorption (XAS), lanthanide luminescence, and vibrational (IR, Raman) spectroscopies. In XAS, X-rays are tuned to excite selectively the *s*- or *p*-shell electrons of metal ions, usually first-row transition metals. Depending on the experiment, XAS can yield the metal ion's oxidation state (X-ray absorption near-edge structure, or XANES) or the distances between the metal ion and atoms within 4 – 5 Å (extended X-ray absorption fine structure, or EXAFS). Nucleobase- and phosphate-bound metal ions may be distinguished readily, due to the higher electron density of phosphorous. Using EXAFS, DeRose and colleagues have obtained evidence suggesting that a Mn^{2+} ion binds oxygen, rather than sulfur, in a phosphorothioate-substituted hammerhead ribozyme (65). Lanthanide ions, most notably Eu^{3+} and Tb^{3+}, undergo distinct *f*-orbital electronic transitions that are sensitive to the coordination environment of the metal ion. In particular, the luminescent lifetimes of these ions vary depending on whether the ions coordinate water molecules (which provide a pathway for luminescence quenching) or RNA ligands. Lanthanide luminescence has been used to detect and characterize metal ion binding in tRNA (66, 67), RNA hairpin loops (68), the U2–U6 spliceosomal RNAs (69), and the hammerhead (70), hairpin (71), and HDV (72) ribozymes. Vibrational spectroscopies can also detect metal ion-induced changes in RNA structure, as well as the coordination environment of specific bound metal ions. Recently, pH-dependent Raman microscopy of HDV ribozyme crystals has provided evidence that a hydrated Mg^{2+} ion binds a G·U wobble pair near the cleavage site (13). Previous work had established that a peak around 323 cm^{-1} in the HDV Raman difference spectrum arose from hydrated Mg^{2+} ions that coordinated at least one non-water ligand (73). By monitoring this Raman signal, the authors have shown that protonation of the catalytic cytosine C75 resulted in the loss of a single inner sphere Mg^{2+} hydrate per HDV molecule. In contrast, substitution of the cleavage site G1 with 7-deazaguanosine (7DG) produced a Raman difference spectrum that lacked both an N7 peak and the inner sphere Mg^{2+} hydrate marker at 323 cm^{-1} (Figure 4A). These observations suggested a model in which a partially hydrated Mg^{2+} ion that functions as the general base in the HDV ribozyme reaction coordinates the N7 of the cleavage site guanosine (Figure 4B).

Computational and database methods

In the context of a three-dimensional structure, certain *in silico* modalities can predict regions within an RNA where metal ions are likely to localize. Such methods may be helpful if the structure is not of sufficient resolution to visualize metal ions, or if the patterns of electron density preclude unambiguous assignment. One approach uses the three-dimensional structure as the basis for calculating solutions to the nonlinear Poisson-Boltzmann equation (NLPB) to determine the molecule's electrostatic potential surface. Locations of highly negative electrostatic potential that may harbor metal ion binding sites are then easily observed (74) (Figure 5). Brownian dynamics algorithms have also been applied that simulate bulk metal ion binding along an RNA's electrostatic potential surface (75). Another program called FEATURE, developed originally to study microenvironments within proteins (76), has been adapted to study metal ion binding sites within RNAs. FEATURE starts with a training set of known metal ion microenvironments within RNA structures and applies these constraints to other RNA structures to predict likely metal ion binding sites (77). The program successfully identified site-bound metal ions observed in crystals of the P4–P6 domain derived from the *Tetrahymena* group I intron, and also predicted additional sites that had not been reported previously.

Web-based databases are also available for studying metal ion binding sites within RNA structures. These include the Metalloprotein Database and Browser (MDB; http://metallo.scripps.edu) (78), the Metals in RNA database (MeRNA; http://merna.lbl.gov) (79), and the Metal Ions in Nucleic Acids database (MINAS; http://www.minas.uzh.ch). The

MDB catalogs all examples within the Protein Data Bank (PDB) of metal ion-ligand interactions occurring within protein and nucleic acid structures. The database is searchable by author, PDB identification number, metal ion, number of ligands, and metal ion-ligand distance, among other parameters. A Java-based applet displays the metal ions and surrounding ligands within a manipulable three-dimensional environment. MeRNA lists all metal ion binding sites in RNA structures deposited in the PDB and the Nucleic Acid Database (NDB). As of 2007, the list comprises over 16,000 metal ions, representing 23 different metal ions within 389 RNA structures. In addition to the search parameters mentioned for the MDB, MeRNA is also searchable by eight different RNA metal ion-binding motifs. The database may be used in conjunction with the Structural Classification of RNA database (SCOR; http://scor.berkeley.edu) (80) to study metal ion binding sites in the context of the overall RNA structure and its tertiary interactions. MINAS was created as a tool to investigate the origin of the selectivity and specificity of nucleic acid metal ion binding sites for metal ions. To that end, the database contains the geometric parameters of every inner and outer sphere-bound metal ion present in over 1,200 nucleic acid structures derived from the PDB and the NDB. Besides inner and outer sphere coordination, users can also search the database for specific coordination environments or combinations of ligands. As stated on their website, the authors hope to classify metal ion binding sites through statistics, and to draw conclusions about the coordination properties of the metal ions involved.

Lanthanide cleavage

Lanthanide ions, notably Tb^{3+} and Eu^{3+}, have been used to map RNA metal ion binding sites through regio-specific hydrolysis of the RNA backbone. These ions compete with Mg^{2+} for metal ion sites on RNA, binding many times more tightly than Mg^{2+} (66, 67). In addition, lanthanide aqua ion pK_a values are close to physiologic pH, allowing micromolar concentrations to induce backbone cleavage in the vicinity of the metal ion site. Following cleavage, the locations of the sites are mapped by fractionating the products on denaturing gels. Lanthanide cleavage maps do not identify catalytic metal ion ligands *per se*, but as with other methods, the maps can narrow the search to specific regions of the ribozyme. Metal ion sites within the group II intron (81), RNase P (82), HDV (72, 83), and hairpin (71) ribozymes have been mapped via lanthanide cleavage. The technique can also be used to monitor RNA folding and the formation of tertiary structure, with higher concentrations of lanthanide ions (micromolar to millimolar) promoting nonspecific hydrolysis in solvent-accessible areas (83–85).

Heavy atom isotope effects

Isotopic substitution is the smallest perturbation that can be made within a catalytic system. Even so, this subtle change can affect the reaction rate and equilibrium significantly, giving rise to kinetic and equilibrium isotope effects, respectively. These effects provide information about the reaction mechanism and the structure of the transition state. Isotope effects are expressed as the ratio of the reaction rates for the lighter isotope compared to the heavier isotope (k_L/k_H). The effect is said to be *normal* if this ratio exceeds unity (favoring the lighter isotope), and *inverse* if it is less than unity (favoring the heavier isotope). In addition, *primary* isotope effects arise from substitution of atoms directly involved in making or breaking bonds, such as nucleophiles and leaving groups. *Secondary* isotope effects, in contrast, result from substitution of atoms that may contribute to transition state structure but do not participate directly in bond formation or cleavage. The magnitude of the effect is proportional to the relative mass difference between the two isotopes. Thus, the effect for hydrogen versus deuterium (a 100% mass difference) is significantly larger than the effect for ^{16}O versus ^{18}O (a 12.5% difference) or for ^{12}C versus ^{13}C (an 8.3%

difference). As a result, detection of isotope effects for atoms other than hydrogen requires extremely precise measurements (≥ 1%) (86).

Two factors contribute to the isotope effect observed experimentally for a given reaction (86–88). A temperature-independent factor (TIF) arises from the difference between the zero point vibrational energies of the chemical bonds involving the two isotopes. Due to the increased mass, the bond to the heavier isotope vibrates at a lower energy level than the bond to the lighter isotope. As a result, formation of the transition state with the heavier isotope requires more activation energy, and hence the TIF is always normal (favoring the lighter isotope). The second contribution to the overall isotope effect reflects the change in bonding experienced by the atom of interest as it proceeds from the ground state to the transition state. This effect is influenced partly by temperature, and therefore is called the temperature-dependent factor (TDF). The TDF can be either normal or inverse, depending on the degree of bonding to the atom in question. In general, a stronger, or “stiffer”, bonding environment arising from bond formation favors the heavier isotope, while a decrease in stiffness (bond cleavage) favors the lighter isotope. The overall isotope effect therefore provides information about the extent of bonding to the reacting atoms in the transition state.

Isotope effects have been used in several instances to study reactions involving solution- or protein-mediated cleavage of model phosphate esters (89–92), as well as proton transfer in some ribozyme reactions (93, 94). The influence of metal ions on the hydrolysis of model phosphate esters has been explored (95–100), but relatively few studies have investigated isotope effects associated with metal ion binding within ribozymes. One notable example from the work of Harris and colleagues (101) extends to RNase P catalysis the results derived from water- and Mg^{2+}-catalyzed hydrolysis of a model phosphate diester. Metal ion binding to nucleophiles generally creates a “stiffer”, more strongly bonded environment that favors heavier isotopes in a reaction (102). Hence, a metal ion-nucleophile interaction should make inverse contributions to the overall isotope effect, a prediction that was observed for Mg^{2+}-catalyzed cleavage of 5’-*p*-nitrophenylphosphate (T5PNP) (101). The isotope effect for T5PNP hydrolysis in $H_2\,^{18}O$ dropped from 1.068 to 1.027 when Mg^{2+} was added, suggesting Mg^{2+} coordination to the ^{18}O nucleophile. In the same study, the authors measured the ^{18}O isotope effect for RNase P catalysis, which requires Mg^{2+} ions and in which water also acts as the nucleophile. The magnitude of the effect (1.030) was very close to that observed for Mg^{2+}-catalyzed cleavage of T5PNP, suggesting that a metal ion coordinates the nucleophilic water in the RNase P reaction.

Aside from the requisite high precision, isotope effect experiments on ribozymes pose an additional challenge with respect to the incorporation of isotopes. The transition states of ribozyme-catalyzed phosphoryl transfer reactions can include 2’-, 3’-, and nonbridging oxygens, yet synthesis of isotopically-enriched nucleotides has been relatively limited and nucleobase-dependent. However, recent studies have reported improved methods for ^{18}O incorporation into nucleotides and phosphoramidites at the 2’ and 3’ positions (103, 104). These molecules should facilitate the investigation of isotope effects and of ribozyme transition state structures.

Nucleotide analog interference mapping (NAIM)

Nucleotide analog interference mapping (NAIM) screens the functionality of specific atoms or groups of atoms at every position of an RNA molecule simultaneously (105). In a NAIM experiment, an RNA is transcribed in the presence of wild-type nucleotides and a nucleoside α-thiotriphosphate. The latter nucleotide contains a modification, either the α-thiophosphate by itself or combined with an atomic substitution elsewhere on the nucleotide. The concentration of nucleoside α-thiotriphosphate is adjusted such that each transcribed RNA

contains one modified nucleotide on average. Following transcription and purification, the pool of RNAs is subjected to some biochemical challenge (selection), such as the ability to fold or perform catalysis. Those RNAs that perform the challenge successfully are isolated, treated with iodine to cleave the phosphorothioate linkages, and fractionated on denaturing gels alongside iodine-treated unselected RNA. Positions where the modification has interfered with the ability of the RNA to perform the challenge appear as gaps in the sequencing ladder.

Since the majority of metal ion-ligand interactions within RNAs involve nonbridging phosphate oxygens (106, 107), NAIM experiments using nucleoside α-thiotriphosphates have been especially effective at locating potential catalytic ligands. Unfortunately, these experiments survey only the R_P nonbridging oxygens, since RNA polymerases incorporate only S_P phosphorothioate diastereomers into the growing transcript. Despite this limitation, however, interference maps can direct the search for catalytic ligands to specific nucleotides. An early investigation of the *Tetrahymena* ribozyme implicated several positions where phosphorothioate substitution interfered with catalysis in the presence of Mg^{2+} alone (108). These positions formed part of the basis for a subsequent search for nonbridging oxygens that coordinated the catalytic metal ions. As later studies showed, the S_P nonbridging oxygens of C208, C262, and A306 bound catalytic ions (109–111), even though each of these positions had been identified initially through R_P phosphorothioate interference.

Metal ion rescue experiments

Metal ion rescue experiments provide a powerful strategy for identifying functional metal ion-ligand interactions within macromolecules. These assays exploit the differential affinities of two or more metal ions for two different ligands. For a given metal ion-ligand interaction critical for some function, substitution of the original ligand with one that interacts weakly with the metal ion would be expected to diminish that function. The subsequent restoration of activity upon addition of a metal ion that binds the substituted atom more strongly suggests that the metal ion-ligand interaction has been reestablished, or "rescued". Thus, the approach isolates individual metal ion-ligand interactions, circumventing the complications of the "sea of metal ions" that surrounds macromolecules. For protein enzymes, metal ion rescue experiments have provided evidence for catalytic involvement of aspartate and glutamate residues within some DNA transposases and integrases (112–116). However, generalized substitution of individual atoms within proteins remains a challenging undertaking (117). Ribozymes, on the other hand, have been especially attractive targets for this technique since both substrates and ribozymes are more amenable to synthetic manipulation. Quantitative metal ion rescue experiments have characterized catalytic metal ion-ligand interactions within the group I (109–111, 118–124) and group II (125–128) introns, the hammerhead ribozyme (129–131), bacterial RNase P (132–139), and the spliceosome (140–142). Crystal structures of hammerhead (31) and group I (15–18) ribozymes have confirmed the validity of the approach, with the majority of the apparent metal ion-ligand interactions agreeing with the biochemical rescue data.

Mg^{2+} ions often facilitate ribozyme catalysis by coordinating oxygen ligands such as 2'-OH groups and bridging and nonbridging phosphate oxygens. In place of oxygen, a metal ion rescue experiment substitutes sulfur or nitrogen (usually as NH_2), two ligands that do not interact particularly well with Mg^{2+}. The rescuing metal ions are transition metals such as Mn^{2+}, Zn^{2+}, Cd^{2+}, or Co^{2+}. The higher polarizability and *d*-orbitals of these metal ions allow them to interact much more strongly with sulfur or nitrogen than Mg^{2+}, which prefers to bind oxygen ligands almost exclusively (143).

To report accurately on the role of a metal ion in a ribozyme reaction, a metal ion rescue experiment must satisfy certain conditions. The assay must monitor the same transition from ground state to transition state, regardless of the presence of an atomic substitution or rescuing metal ion. The altered substrate-ribozyme combination may change the initial ground state of the reaction, or accelerate a non-chemical step unexpectedly. Identical reaction conditions may yield a log-linear pH dependence for the wild-type reaction, and a pH-independent profile for the modified reaction. Therefore, care must be taken to identify experimental conditions under which the chemical step of the reaction is rate-limiting for all modifications, substrates, and metal ions employed. This requires a rigorous thermodynamic and kinetic analysis of the reaction, including knowledge of substrate and cofactor binding parameters, relevant conformational changes, and how different modifications and conditions affect each individual step of the pathway.

In addition, any non-specific effects of the rescuing metal ion must be considered. Even under conditions in which chemistry is rate-limiting, a rescuing metal ion may confer an inherent catalytic advantage to the reaction. Alternatively, some rescuing metal ions (notably Cd^{2+}) may inhibit a reaction at sufficiently high concentrations (124). To control for these effects, separate experiments must monitor both the wild-type and modified reactions in the presence of Mg^{2+} alone and with the rescuing metal ion. The rates of these reactions are then used to calculate a relative rate, k^{rel}, that controls for the non-specific effects of the rescuing metal ion. For a ribozyme system in which sulfur or nitrogen (S/N) substitutes for an oxygen ligand (O), k^{rel} is given by the expression

$$k^{rel} = \frac{\frac{k_{S/N}^{M^{2+}}}{k_{S/N}^{Mg^{2+}}}}{\frac{k_{O}^{M^{2+}}}{k_{O}^{Mg^{2+}}}} \quad (1)$$

where M^{2+} is the rescuing metal ion and each k is the rate of the reaction in the presence of either Mg^{2+} alone or Mg^{2+} plus M^{2+}. The magnitude of the rescue is therefore proportional to the M^{2+} rate acceleration of the modified reaction divided by the M^{2+} acceleration inherent to the wild-type reaction.

An important point regarding the interpretation of these experiments is that a lack of rescue does not imply the absence of metal ion coordination by the original ligand. The physicochemical properties of the substitution or the rescuing metal ion may preclude restoration of a disrupted metal ion-ligand interaction. Sulfur, for example, is bulkier than oxygen, and a phosphorothioate P-S bond is significantly longer than the corresponding P-O bond (1.9 Å vs. 1.5 Å, respectively). Phosphorothioate and all-oxygen linkages also differ with respect to their charge distribution (144), electronegativity, and ability to accept hydrogen bonds (145). Thus, depending on the structural and chemical context, phosphorothioate substitution may introduce a perturbation that softer metal ions cannot overcome, even though the original ligand coordinated a metal ion. In some cases, the sulfur atom may actually displace catalytic metal ions from the active site (146). In addition, the rescuing metal ions differ from Mg^{2+} with respect to size and coordination geometry. While Mg^{2+} and Mn^{2+} have similar ionic radii (0.72 Å vs. 0.67 Å, respectively), the more thiophilic Cd^{2+} ion is significantly larger (0.95 Å). Zn^{2+} is more thiophilic than Mn^{2+} and at 0.74 Å is closer in ionic radius to Mg^{2+}, but may adopt a tetrahedral rather than an octahedral coordination geometry depending on the structural context. Each of these caveats regarding the substitution and the rescuing metal ion must be considered when a metal ion rescue experiment yields a negative result.

Metal ion rescue in practice: The *Tetrahymena* GROUP I intron catalytic site

The protozoan *Tetrahymena thermophila* contains a self-splicing group I intron within the gene encoding the 26S rRNA (147). A shortened form of this intron (Figure 6) catalyzes a phosphotransesterification reaction between an exogenous guanosine molecule and an oligonucleotide substrate that forms base pairs with the ribozyme (148):

$$CCCUCUA+G \rightarrow CCCUCU+GA$$

In vitro, the ribozyme is active at millimolar concentrations of Mg^{2+} or Mn^{2+}, whereas neither Ca^{2+} nor monovalent ions alone support catalysis (149). Kinetic analyses of the reaction (1, 150–152) support the scheme shown in Figure 7, in which substrate binding occurs via the formation of two distinct intermediates. In the *open complex*, the substrate base pairs with the ribozyme to form the P1 helix. This species then undergoes a conformational change ("docking") to form the *closed complex*, in which the P1 helix forms tertiary contacts with the ribozyme core. Metal ion rescue experiments based upon this kinetic framework have led to the development of a detailed model of the interactions between divalent metal ions and atoms of the substrate and ribozyme in the transition state (Figure 6C). The following sections describe some of the methods and strategies used to obtain the data that support this model.

Metal A coordinates the 3' leaving group of the substrate

Piccirilli *et al.* identified the first metal ion-ligand interaction within the *Tetrahymena* ribozyme that participates directly in the catalytic mechanism. Using a metal ion specificity switch experiment, they showed that a divalent metal ion (M_A) coordinates the 3' oxygen leaving group of the oligonucleotide substrate (118) (Figure 8A). This discovery depended in part upon two key experimental results. One was the ability to synthesize deoxyribonucleotides containing a 3' phosphorothiolate linkage. This was accomplished through the efforts of Vyle and Cosstick, who prepared the 3'-S-phosphorothioamidite of thymidine and used it to produce a dithymidine 3'-S dinucleotide (153). Subsequent work described the incorporation of the phosphorothioamidite into longer deoxyribonucleotides via automated solid-phase synthesis (154). The other relevant result was the observation that the *Tetrahymena* ribozyme could cleave an all-DNA oligonucleotide substrate, albeit with weaker substrate binding and decreased rate constants compared to the all-RNA substrate (155). Importantly, while substrate binding and product release limited the reaction of the all-RNA substrate, the all-DNA substrate reacted such that the chemical step was rate-limiting at all concentrations of guanosine and substrate.

To conduct the experiment, Piccirilli *et al.* first synthesized the DNA substrate $d(CCCUCU_{3'X}A)$, where X is either oxygen or sulfur. In the presence of 12 mM Mg^{2+}, the reactivity of the sulfur substrate in the *Tetrahymena* ribozyme reaction was about 1000-fold lower than the reactivity of the oxygen substrate. Because both substrates reacted from the same ground state under conditions in which chemistry was rate-limiting, this differential reactivity arose from a defect in the chemical step, rather than from a conformational change. Also, the sulfur substitution did not affect substrate binding to the ribozyme, as was shown by direct K_d measurements using native gels. Increasing the Mg^{2+} concentration accelerated the reaction of both substrates, but did not affect the 1000-fold relative catalytic defect. In contrast, in the presence of 10 mM Mg^{2+} and 2 mM Mn^{2+}, the ribozyme cleaved the sulfur substrate only 8-fold more slowly than the oxygen substrate. The presence of Mn^{2+} did increase the reaction rate for the oxygen substrate by about 3-fold, likely due to enhancement of substrate docking into the closed complex (156). However, the 400-fold increase in the cleavage rate of the sulfur substrate in the presence of Mn^{2+} suggested

strongly that a process other than nonspecific Mn^{2+} stimulation was at work. The additional observation that higher Mg^{2+} concentrations could suppress the Mn^{2+}-stimulated reaction of the sulfur substrate strengthened the conclusion that a divalent metal ion coordinates the 3' leaving group.

Metal B coordinates the 3'-OH nucleophile of guanosine

In a seminal 1993 paper, Steitz and Steitz proposed a generalized two-metal ion mechanism for RNA-catalyzed phosphotransesterification reactions (157). In their scheme, one metal ion activates an incoming oxygen nucleophile, a second metal ion stabilizes the leaving group oxygen, and both metal ions coordinate one of the nonbridging phosphate oxygens. These interactions are suggested to stabilize the developing negative charges on the atoms within the pentavalent transition state, analogous to the role metal ions play in catalysis by protein enzymes like DNA polymerase (158, 159) and alkaline phosphatase (160). For the *Tetrahymena* ribozyme, M_A had been identified as the metal ion that stabilized the 3'-oxygen leaving group. Whether a second metal ion activated the 3'-OH of the guanosine nucleophile to complete a two-metal ion mechanism was unknown.

Following the logic of the experiments that found M_A, the strategy to determine whether a metal ion coordinates the guanosine 3'-OH nucleophile in the transition state might have employed 3'-thioguanosine. However, as sulfur is a relatively poor nucleophile at phosphorous centers (161), the experimental assay instead monitored the reverse reaction according to

$$\mathrm{CCCUCU{+}I_{3'X}U} \quad \mathrm{CCCUCUU{+}I_{3'XH}}$$

where X is either oxygen or sulfur, and I is inosine (120). In this reaction, the terminal 3'-OH of CCCUCU attacks the phosphorous atom of the dinucleotide, releasing free inosine with either a 3' oxygen or 3' sulfur leaving group. By the principle of microscopic reversibility, a metal ion coordinating the 3' leaving group in the reverse reaction would coordinate the 3' nucleophile in the forward reaction. The dinucleotide contained inosine at the 5' position because at the time, the synthesis of the 3'-phosphorothiolate linkage was easier with inosine than with guanosine. Previous studies of this reaction found that inosine could substitute for guanosine at the 5' position of the dinucleotide (162, 163). Although a thermodynamic and kinetic framework for the reverse reaction had not been established fully, the observation that the reactions occurred with a log-linear pH dependence from pH 5.5 to 7.0 was consistent with the chemical step being rate-limiting.

In the presence of 110 mM Mg^{2+} at pH 7.0, only $I_{3'O}U$ was a substrate in the reverse reaction, and no detectable activity was observed with $I_{3'S}U$. As in the M_A rescue experiments, the lack of $I_{3'S}U$ cleavage did not result from reduced binding to the ribozyme. Adding softer divalent metal ions stimulated the reaction of $I_{3'S}U$, but only Cd^{2+} produced a true metal ion rescue, increasing the reaction rate of $I_{3'S}U$ significantly above that of $I_{3'O}U$. Again, analogous to the M_A experiments, increasing concentrations of Mg^{2+} (from 0 – 100 mM, in a background of 18.5 mM Mg^{2+} and 2 mM Cd^{2+}) inhibited $I_{3'S}U$ cleavage, suggesting that Mg^{2+} competed with Cd^{2+} for the site of rescue. The metal ion (M_B, Figure 8B) interacts with the leaving group in the transition state for the reverse reaction. Therefore, by the principle of microscopic reversability, this metal ion must interact with the nucleophile in the forward reaction.

Metal C coordinates the 2'-OH of guanosine

Around the same time that the work on M_B was being performed, Strömberg and colleagues reported an interaction between a divalent metal ion and the 2'-OH of the guanosine nucleophile (119). The evidence arose from assays in which 2'-deoxy-2'-aminoguanosine ($G_{2'NH_2}$) replaced guanosine in the reaction of the group I intron derived from the bacteriophage T4 *nrdB* gene (164, 165). The experiments monitored the first step of splicing of a pre-mRNA containing 22 nucleotides of exon 1, the 598-nucleotide intron, and 200 nucleotides of exon 2. In the presence of Mg^{2+} alone (4 mM $MgCl_2$, 40 mM PIPES-KOH pH 7.2, 60 mM KCl), the reaction rate with $G_{2'NH_2}$ was 30-fold lower than with guanosine, although the binding constants for both forms of guanosine were similar. Chemistry for this reaction appeared to be rate-limiting, since both k_{cat} and (k_{cat}/K_M) were log-linearly dependent on pH. A mixture of 4 mM Mg^{2+} and 0.9 mM Mn^{2+} stimulated the reaction rate with $G_{2'NH_2}$ about 6-fold, while 0.1 mM Zn^{2+} increased the rate 35-fold above the Mg^{2+}-only rate. These observations, among others, led the authors to hypothesize that the 2'-OH of guanosine positioned a metal ion so that it could activate the nearby 3'-OH nucleophile in the first step of splicing. However, the study did not control adequately for the nonspecific effects of the rescuing metal ions, since the total divalent metal ion concentration was not always held constant. The authors did note that the optimal Mn^{2+} concentration for the reaction involving $G_{2'NH_2}$ was 0.3 – 1 mM, with Mg^{2+} added up to a total divalent metal ion concentration of 4 mM. The corresponding reaction rate for guanosine, however, was not reported.

In subsequent work, Shan and Herschlag provided further evidence for an interaction between a metal ion and the 2' moiety of guanosine. First, they confirmed that both Mn^{2+} and Zn^{2+} rescued the reaction of the *Tetrahymena* ribozyme when $G_{2'NH_2}$ replaced guanosine (122). In addition, they developed a thermodynamic and kinetic framework to analyze the effects of Mn^{2+} binding on each individual step in the reaction pathway: binding to free ribozyme (E), to the enzyme-substrate complex (E·S), and to the ternary complex (E·S·G or E·S·$G_{2'NH_2}$). The results showed that a single Mn^{2+} ion rescued the reaction involving $G_{2'NH_2}$. The chief effect of this ion was to increase the affinity of $G_{2'NH_2}$ for the E·S complex, and of substrate (S) for the E·$G_{2'NH_2}$ complex. In contrast, the ion did not affect the affinity of G for E·S, or of S for E·G, nor did it alter the binding of G, $G_{2'NH_2}$, or S to the free ribozyme E. The ion also had little effect on the rate of the chemical step starting from either the E·S·G or the E·S·$G_{2'NH_2}$ ternary complex. Higher concentrations of Mg^{2+} decreased the affinity of the rescuing Mn^{2+} ion for E and E·S, indicating that Mg^{2+} competed with Mn^{2+} for binding at the site of rescue.

Taken together, these observations supported a transition state interaction between the 2' moiety of guanosine and a divalent metal ion (M_C, Figure 8C). Furthermore, the apparent cooperativity of $G_{2'NH_2}$ or S binding to E·S or E·$G_{2'NH_2}$, respectively, in the presence of Mn^{2+} suggested that M_C provided a structural bridge between guanosine and the substrate. This bridge required the presence of the reactive phosphate linkage, since Mn^{2+} had no effect on the affinity of $G_{2'NH_2}$ for the enzyme-product complex E·P (122). The authors noted that this interaction might help to align guanosine within the catalytic site for optimal in-line attack of the 3'-OH on the scissile phosphate. In fact, later work showed that interactions between S and M_C drive a conformational change that facilitates the binding of guanosine to the ribozyme (166).

Do three separate metal ion-ligand interactions arise from three distinct metal ions?

At this point, metal ion rescue experiments had identified three different catalytic interactions between divalent metal ions and specific atoms of the oligonucleotide substrate and guanosine nucleophile. However, these experiments had not been designed to determine

the number of metal ions responsible for these contacts. One possibility was that three distinct metal ions (M_A, M_B, and M_C) bound the 3' leaving group, the guanosine 3'-OH, and the guanosine 2'-OH, respectively, in the transition state. Or, M_C might align guanosine through its 2'-OH and simultaneously activate the 3'-OH nucleophile, without the need for an additional M_B. Counting the number of divalent ions within the catalytic site required a strategy that could monitor the effects of individual catalytic metal ion-ligand interactions on the reaction. The Herschlag and Piccirilli groups devised a way to discriminate among individual metal ions that bound to the three known sites A, B, and C. The method, called thermodynamic fingerprint analysis (TFA), involved measuring the affinities of rescuing metal ions for each site on the free ribozyme (E) (121). Which site was being interrogated depended upon the specific substrate modification used in the reaction. For example, to obtain the affinity of a rescuing Mn^{2+} ion for site A, a substrate containing oxygen or sulfur as the 3' leaving group ($S_{3'X}$, where X = O or S) was used. The experiment followed the reaction of $S_{3'X}$ first in the presence of 10 mM Mg^{2+}, and then in 10 mM Mg^{2+} with increasing concentrations of Mn^{2+}. The overall kinetic framework is shown in Scheme 1, where K^{Mn} is the affinity of the rescuing Mn^{2+} ion and k^{rel} is the relative rate constant of the oxygen and sulfur substrate reactions ($k^{rel} = k_{3'S}/k_{3'O}$) performed in Mg^{2+} alone or with added Mn^{2+}.

The relative reaction rates were used to control for any nonspecific effects of Mn^{2+} (or any other rescuing metal ion). The observed rate constant k^{rel}_{obs} for the reaction shown in Scheme 1 depends upon the fraction of free enzyme with a metal ion bound to site A:

$$k^{rel}_{obs} = k^{rel}_{Mg}\left\{\text{fraction}^{Mg_A\bullet E}\right\} + k^{rel}_{Mn}\left\{\text{fraction}^{Mn_A\bullet E}\right\} \quad (2)$$

Substituting for $\{\text{fraction}^{Mg_A\bullet E}\}$ and $\{\text{fraction}^{Mn_A\bullet E}\}$ from the kinetic pathway in Scheme 1 yields:

$$k^{rel}_{obs} = k^{rel}_{Mg}\frac{K^{Mn}}{[Mn^{2+}]+K^{Mn}} + k^{rel}_{Mn}\frac{[Mn^{2+}]}{[Mn^{2+}]+K^{Mn}} \quad (3)$$

The affinity of the rescuing Mn^{2+} ion for site A, K^{Mn}, was then obtained by plotting k^{rel}_{obs} versus $[Mn^{2+}]$ and fitting the data to Equation 3, with K^{Mn} as a fitted parameter (Figure 9). In the absence of Mn^{2+}, k^{rel}_{obs} equals k^{rel}_{Mg}, the relative rate constant for the reaction of $S_{3'X}$ in Mg^{2+} alone. The addition of Mn^{2+} accelerates k^{rel}_{obs} according to Equation 3, up to a saturation value of k^{rel}_{Mn}. Thus, the plot depicts the Mn^{2+}-dependent *stimulation* of k^{rel}_{obs}, associated with an affinity K^{Mn} of the rescuing Mn^{2+} ion for metal site A. This affinity is a thermodynamic fingerprint, a unique signature, associated with Mn^{2+} rescue at site A, for the reaction shown in Scheme 1 under a specific set of conditions. Similar methods were used to obtain the affinities of rescuing metal ions for sites B and C, in the context of the appropriate substrate modifications.

Importantly, these experiments were designed to monitor Mn^{2+} binding to the *free* ribozyme in the starting ground state. This ensured that the single-atom modifications of the substrate or guanosine did not affect the apparent affinities of Mn^{2+} ions for the ribozyme. Rescue then occurred due to the transition state interaction between Mn^{2+} and the modification. Because, by definition, the transition state exists only transiently, the modifications did not affect the observed Mn^{2+} affinities (121). For modifications involving the substrate (such as $S_{3'O}$ or $S_{3'S}$), this was accomplished by employing substrates that reacted starting from the open complex. In the open complex, the substrate has not yet docked into the catalytic core,

and therefore cannot affect the affinities of the catalytic Mn^{2+} ions for the free ribozyme. For modifications involving guanosine (such as $G_{2'NH_2}$), the experiments monitored the reaction E·S + G → products, in which the modified guanosine was not bound in the starting ground state. As a result, Mn^{2+} affinities obtained from experiments involving different substrate modifications could be compared directly. If a Mn^{2+} ion rescued one modification with the same affinity as it did a different modification, the simplest interpretation would be that the same metal ion mediates the interaction with both modifications. On the other hand, two different Mn^{2+} affinities would imply that distinct metal ions rescue each modification.

By using TFA, three different affinities were found for the binding of rescuing Mn^{2+} ions to sites A, B, and C on the *Tetrahymena* ribozyme (121, 122). M_A rescued the reaction of $S_{3'S}$ with an affinity of 0.8 ± 0.2 mM (30 °C, 50 mM NaEPPS pH 7.9, 10 mM $MgCl_2$), M_B rescued the reaction of $G_{3'S}U$ with an affinity of 7 ± 1 mM (30 °C, 50 mM NaMES pH 6.3, 10 mM $MgCl_2$), and M_C rescued the reaction involving $G_{2'NH_2}$ with an affinity of 0.28 ± 0.06 mM (identical conditions as for M_A). The closeness of the affinities of M_A and M_C prompted additional experiments to determine if these metal ions were truly distinct.

Running the reaction in the presence of both $S_{3'S}$ and $G_{2'NH_2}$yielded plots of k_{obs}^{rel} consistent with a model in which two separate ions rescue the reaction. The data therefore supported the existence of at least three separate metal ions binding within the catalytic site of the *Tetrahymena* ribozyme during the course of its reaction.

Interactions with the *pro-S*$_P$ nonbridging oxygen of the scissile phosphate

The two nonbridging oxygens at the scissile phosphate had been tested earlier as possible divalent metal ion ligands within the *Tetrahymena* catalytic site. Of the two, the *pro-S*$_P$ nonbridging oxygen seemed more likely to play this role since sulfur substitution of this oxygen reduced the reaction rate about 1000-fold (163). In comparison, sulfur substitution of the *pro-R*$_P$ oxygen produced only a 2.5-fold rate decrease (167). However, the addition of softer divalent metal ions did not fully rescue the reaction involving either of these substitutions (163, 167). Evidence from model compound studies suggested that the modest catalytic defect due to sulfur substitution of the *pro-R*$_P$ oxygen did not result from disruption of metal ion coordination (167). In contrast, the significant loss of activity upon substitution of the *pro-S*$_P$ oxygen with sulfur hinted at possible metal ion involvement, despite the negative rescue result.

Piccirilli and colleagues resolved the role of the *pro-S*$_P$ nonbridging oxygen by testing the reactivity of a substrate with sulfur substitutions at both the *pro-S*$_P$ nonbridging and 3' leaving group oxygens (123). In a mixture of Mg^{2+} and Mn^{2+}, this phosphorodithioate substrate ($S_{3'S,P\text{-}S}$) reacted more slowly than control substrates containing either a single 3' bridging sulfur or a 3' bridging sulfur and a *pro-R*$_P$ nonbridging sulfur. In contrast, the substitution of Zn^{2+} for Mn^{2+} restored the reactivity of $S_{3'S,P\text{-}S}$ to a level comparable to that of the single 3' sulfur substrate. This result suggested that a metal ion or ions interacted with both the 3' bridging and the *pro-S*$_P$ nonbridging oxygens in the transition state. The inability of Mn^{2+} or Zn^{2+} to rescue the reaction of the original *pro-S*$_P$ sulfur substrate ($S_{P\text{-}S}$) was attributed to a possible geometric distortion caused by the presence of sulfur. Unlike $S_{P\text{-}S}$, $S_{3'S,P\text{-}S}$ presented two sulfur atoms that could interact more favorably with the tetrahedral coordination geometry of Zn^{2+} than with the octahedral Mn^{2+}. Although this work established that the *pro-S*$_P$ nonbridging oxygen interacts with a metal ion, whether this newly discovered ligand interacted with a fourth metal ion, or with one of the metal ions identified previously (M_A, M_B, or M_C), remained unclear (Figure 10A). The lack of Mn^{2+} rescue in the reaction of $S_{3'S,P\text{-}S}$ precluded the use of standard TFA, since the M_A, M_B, and M_C fingerprints represent apparent Mn^{2+} affinities. In principle, TFA might have been applied to the reactions involving $S_{3'S,P\text{-}S}$ by measuring the Cd^{2+} dependences of rescue of

the M_A, M_B, and M_C reactions. However, unlike the Mn^{2+} rescue profiles, the Cd^{2+} rescue profiles did not exhibit saturation behavior within the Cd^{2+} concentration range above which Cd^{2+} strongly inhibits the reaction. As a result, Cd^{2+} fingerprints analogous to those obtained with Mn^{2+} could not be determined. Plots of log k_{rel} versus log [Cd^{2+}], where k_{rel} represents the observed rate constant for reaction of $S_{3'S,P\text{-}S}$ relative to unmodified substrate, were linear with a slope (n) of 2, implying that at least two Cd^{2+} ions mediate rescue of $S_{3'S,P\text{-}S}$ (124) (Figure 11). In contrast, Cd^{2+} rescue profiles for the reaction of $S_{3'S}$ relative to the unmodified substrate exhibited a shallower Cd^{2+} concentration dependence (n = 1), consistent with a single metal ion (M_A) involved in the rescue. As $S_{3'S,P\text{-}S}$ contains a 3' sulfur leaving group, presumably the same Cd^{2+} ion that mediated rescue of $S_{3'S}$ (M_A) contributed to rescue of the dithioate by coordinating to the sulfur leaving group. The second Cd^{2+} ion likely interacted with the nonbridging atom in the transition state and could bind at the M_B or M_C site, or at a previously unidentified binding site.

To assess whether the second Cd^{2+} ion involved in the rescue of $S_{3'S,P\text{-}S}$ bound in the M_B or M_C site, Shan *et al.* performed competition experiments with Mn^{2+} (124). Although Mn^{2+} does not rescue the reaction of $S_{3'S,P\text{-}S}$, it does bind to the M_A, M_B, and M_C binding sites with known affinities. Therefore, if the two Cd^{2+} ions involved in rescue of $S_{3'S,P\text{-}S}$ bound at these sites, then Mn^{2+} would be expected to inhibit rescue by competing with Cd^{2+} for binding. One of the rescuing Cd^{2+} ions presumably bound in the M_A site (to mediate the interaction with the leaving group). If the second Cd^{2+} involved in the rescue of $S_{3'S,P\text{-}S}$ bound to the M_B site, then Mn^{2+} would inhibit rescue by competing with Cd^{2+} for binding to the M_A and M_B sites. In contrast, if the second Cd^{2+} involved in the rescue of $S_{3'S,P\text{-}S}$ bound to the M_C site, then Mn^{2+} would inhibit rescue by competing with Cd^{2+} for binding to the M_A and M_C sites. Because Mn^{2+} bound to the M_C site 10-fold more strongly than to the M_B site, the model involving the M_A and M_C sites predicted greater competition from Mn^{2+} than did the model involving the M_A and M_B sites. The competition experiments showed that Mn^{2+} inhibited the Cd^{2+}-stimulated rescue of $S_{3'S,P\text{-}S}$ with a significantly steeper concentration dependence than predicted from the model involving the M_A and M_B sites. Instead, the Mn^{2+} competition data matched those predicted from the model in which Mn^{2+} competes with Cd^{2+} ions bound at the M_A and M_C sites (Figure 12). These findings led to a working model in which two Cd^{2+} ions rescue the reaction of $S_{3'S,P\text{-}S}$. One bound at the M_A site to stabilize the leaving group, while another bound at the M_C site to interact with the nonbridging atom and the guanosine 2'-OH.

A simple prediction of this model is that the M_C site can bind Cd^{2+}. The reaction of $G_{2'NH_2}$ provided a means to probe Cd^{2+} occupancy of the M_C site. Consistent with the model, Cd^{2+} rescued the reaction involving $G_{2'NH_2}$ relative to the reaction involving guanosine with a log-linear dependence of unit slope, suggesting that a single Cd^{2+} ion binds to the M_C site to stimulate the reaction of $G_{2'NH_2}$ (Figure 13). As a further test of the hypothesis that M_C coordinated the *pro-*S_P nonbridging oxygen, the authors monitored the Cd^{2+} concentration dependence of the reaction of $S_{3'S,P\text{-}S}$ with $G_{2'NH_2}$ relative to the reaction of unmodified S with guanosine. If M_C mediated interactions with both the *pro-*S_P nonbridging oxygen and the guanosine 2'-OH, then two Cd^{2+} ions would have been expected to rescue the reaction of $S_{3'S,P\text{-}S}$ with $G_{2'NH_2}$ relative to the corresponding reactions involving unmodified substrates. One Cd^{2+} ion would populate the M_A site to coordinate the 3' sulfur leaving group, while a second would populate the M_C site and interact with both the nonbridging sulfur atom of $S_{3'S,P\text{-}S}$ and the 2' amino group of $G_{2'NH_2}$. In contrast, if a metal ion distinct from M_C mediated the interaction with the nonbridging atom, then three metal ions would be involved in the rescue of $S_{3'S,P\text{-}S}$ in the presence of $G_{2'NH_2}$. The concentration dependence of both Cd^{2+}- and Zn^{2+}-mediated rescue of this reaction showed that only two ions were responsible for rescue, further supporting the proposed M_C-*pro-*S_P oxygen interaction (Figure 14).

Additional experiments addressed the unresolved question of why softer metal ions had failed to rescue the reaction of $S_{P\text{-}S}$. Although it is softer than Mg^{2+}, Mn^{2+} prefers to bind oxygen rather than sulfur (143), and rescue of $S_{P\text{-}S}$ by Mn^{2+} would require formation of two Mn^{2+}-sulfur interactions (Mn^{2+}_A and Mn^{2+}_C). On the other hand, Cd^{2+} rescue of the $S_{P\text{-}S}$ reaction would require the formation of two unfavorable Cd^{2+}-oxygen interactions (to the 3' leaving group oxygen and the guanosine 2'-OH). Thus, Cd^{2+} might not be expected to rescue the reaction of $S_{P\text{-}S}$ very efficiently, especially considering that Cd^{2+} could not saturate sites A or C even when $S_{3'S,P\text{-}S}$ was used as the substrate. If Cd^{2+} could rescue the reaction of $S_{P\text{-}S}$, it should do so at high concentrations and involve the binding of two Cd^{2+} ions. As predicted, Cd^{2+} did rescue the reaction of $S_{P\text{-}S}$ at concentrations up to 15 mM, with a concentration dependence of two rescuing Cd^{2+} ions.

Functional identification of ribozyme ligands that position the catalytic metal ions

Up to this point, each of the catalytic metal ions that had been identified in the *Tetrahymena* ribozyme coordinated atoms of the oligonucleotide substrate. In contrast, none of the functional groups on the ribozyme itself that positioned these ions were known. As the most likely ligand candidates, the nonbridging phosphate oxygens of several conserved nucleotides within the catalytic core received special attention. An earlier NAIM study had found that phosphorothioate substitution of a number of *pro-R*$_P$ nonbridging oxygens inhibited splicing, and that Mn^{2+} could rescue the reaction of some of these sulfur-substituted ribozymes (108). This study did not explore the precise nature of this rescue, nor could it provide any information about the *pro-S*$_P$ nonbridging oxygens. However, coupled with phylogenetic analysis of the group I intron catalytic core (168) and results from other analog-interference experiments (169, 170), the NAIM data provided a strong starting point for a ligand search.

Strobel and colleagues provided evidence for one of these ligands, the *pro-S*$_P$ nonbridging oxygen of C208 (C208 S_P) (109) (Figure 15A). Relying on a model of the *Tetrahymena* catalytic site (169), they singled out five positions as potential ligands, and constructed the ten corresponding phosphorothioate ribozymes (R_P and S_P). This required dividing the full-length ribozyme into three pieces – a synthetic oligonucleotide containing the phosphorothioate, and two transcribed flanking RNAs. The phosphorothioate oligonucleotides were first separated into R_P and S_P diastereomers by using reversed-phase HPLC. These were then joined to the flanking RNAs by hybridization with bridging DNA splints followed by incubation with DNA ligase (171). Of the ten constructed ribozymes, four showed substantial reductions in reactivity compared to the unmodified ribozyme, but partial Mn^{2+} rescue was observed only for the C208-S_P ribozyme. Subsequent experiments tested the ability of this ribozyme to cleave substrates containing either 3' phosphorothiolate or *pro-S*$_P$ phosphorothioate modifications. By analogy to previous work, it was thought that thiophilic metal ions like Cd^{2+} or Zn^{2+} would rescue the reaction more efficiently in the context of the double sulfur substitution (ribozyme and substrate). While neither Mn^{2+} nor Zn^{2+} rescued the reaction of either sulfur substrate in the context of the C208-S_P ribozyme, Cd^{2+} stimulated both reactions by 70- to 100-fold. Since M_A was known to coordinate both the 3' leaving group and the scissile *pro-S*$_P$ nonbridging oxygen in the transition state, the authors concluded that C208 S_P was a ligand for M_A.

In the absence of thermodynamic fingerprints or the dependence of k^{rel} on the rescuing metal ion concentration, the *range* of metal ions that confers rescue can provide a qualitative approach to link catalytic metal ions to their ligands within the ribozyme. For example, in the *Tetrahymena* ribozyme, incorporation of the S_P phosphorothioate at residue C208 inhibited reaction of the unmodified substrate in Mg^{2+}. Mn^{2+} and Zn^{2+} rescued this effect, but Cd^{2+} did not. However, when the mutant ribozyme was assayed using a substrate containing a 3' phosphorothiolate at the cleavage site, Cd^{2+}, but neither Mn^{2+} nor Zn^{2+},

could rescue the reaction (109). Phosphorothioate substitutions at other positions in the ribozyme did not show this behavior. These results functionally linked the C208 *pro-*S_P phosphorothioate to the 3' phosphorothiolate in the substrate, suggesting that the C208 *pro-*S_P oxygen within the ribozyme provides a ligand to the catalytic metal ion that stabilizes the 3' oxygen leaving group. In-depth quantitative and structural analyses later confirmed this interaction. Thus, functional linkage between groups may be inferred when the combination of modifications leads to rescue behavior distinct from that of either modification alone.

The Herschlag and Piccirilli groups used the concentration dependence of k^{rel} on Cd^{2+} as a signature to identify ligands for the catalytic metal ions. Prior to the publication of the group I crystal structures, they combined substrate atomic mutagenesis with site- and stereospecific phosphorothioate substitutions at six sites within the J6/7 and P7 regions of the ribozyme to identify the ligands to M_A, M_B, and M_C. They tested whether Cd^{2+}, a thiophilic metal ion that, like Mg^{2+}, can adopt octahedral coordination geometry, stimulated the catalytic activity of the phosphorothioate-containing ribozymes in the reaction of G with $S_{3'O}$. Under conditions of saturating E and G, they found that several of the phosphorothioates significantly affected catalysis. However, upon addition of 0.1 – 1.0 mM Cd^{2+}, only one of the variant ribozymes, the C262-S_P variant, experienced significant stimulation, suggesting that Cd^{2+} may form a functionally important interaction with the sulfur at position C262. They used the modified substrates that report on the M_A, M_B, and M_C sites (described above) to ascertain whether the C262 phosphorothioate affected the rescue behavior. If the C262 S_P phosphorothioate directly interacted with a Cd^{2+} ion bound in the M_A, M_B, or M_C sites, they expected that the stronger Cd^{2+}-sulfur interaction (compared to the Cd^{2+}-oxygen interaction in the unmodified ribozyme) would shift the metal rescue profile toward lower Cd^{2+} concentrations compared to the corresponding rescue profile using the unmodified ribozyme. The M_A and M_B rescue profiles remained essentially unaffected by the C262-S_P phosphorothioate. In contrast, the M_C rescue profile (using $G_{2'NH_2}$ as the modified substrate) shifted such that 16-fold lower Cd^{2+} concentrations were required to achieve the same level of rescue as with the unmodified ribozyme. The observation that the C262-S_P phosphorothioate shifted the M_C rescue profile, but not the M_A and M_B profiles, to lower Cd^{2+} concentrations suggested that the sulfur atom interacted directly with the Cd^{2+} ion binding at the M_C site (Figure 15B). Further independent tests supported this model, as did the available crystal structures (see below). Recently, Forconi *et al.* extended this approach to identify two additional ligands for M_A (the *pro-*S_P nonbridging oxygens of A304 and A306) (111) (Figure 15C), verifying interactions inferred from the *Azoarcus* crystal structures. As of this writing, no ligands for M_B have been identified.

Comparison with structural data

Most of the preceding experiments were conducted in the absence of high-resolution structural information. During the transition of the investigation from defining substrate ligands to defining ribozyme ligands, crystal structures of three group I introns emerged, providing for the first time a structural framework with which to evaluate more than a decade of functional experiments. The agreement between the structural and biochemical models is striking. The structures show that nearly all of the predicted ligands are located in close proximity to metal ions residing within the catalytic site. While the resolution of the structures is not sufficient to view Mg^{2+} ions directly, their positions have been inferred based on anomalous scattering maps of heavy metal ion derivatives.

In terms of inferring catalytic interactions, the most recent structure of the *Azoarcus* group I ribozyme (18) likely provides the information relevant to the catalytic mechanism. The 3.4-Å structure captures the ribozyme just after the first step of splicing, with both exons poised for ligation and riboguanosine bound at the 3' splice site. Two Mg^{2+} ions, designated M_1 and M_2, are modeled into the catalytic site based on Yb^{3+} and Mn^{2+} soaks (Figure 16). M_1

makes apparent inner sphere contacts with the 3' oxygen of dT_{-1} (the leaving group in the forward reaction), and the *pro-R*P nonbridging oxygen of the scissile phosphate (corresponding to the *pro-S*P oxygen in the forward reaction). In addition, the *pro-S*P nonbridging oxygens of C88, G170, and A172 (*Tetrahymena* nucleotides C208, A304, and A306, respectively) all lie within inner sphere coordination distance of M_1. A possible outer sphere sixth ligand, the *pro-S*P oxygen of U173 (*Tetrahymena* U307), is also present, although the functional significance of this interaction is unclear (111). This set of ligands suggests that M_1 corresponds to M_A. M_2, on the other hand, appears to correspond to M_C. It lies within 2.2 Å of the 2'-OH of ωG (corresponding to the 2'-OH of the guanosine nucleophile in the forward reaction), the *pro-R*P nonbridging oxygen of the scissile phosphate, and the *pro-S*P nonbridging oxygen of G128 (*Tetrahymena* C262). In addition, the *pro-R*P nonbridging oxygen of A172 appears to contact M_2 via inner sphere coordination, and initial rescue data support the existence of this interaction in *Tetrahymena* (172). Interestingly, M_2 also resides 2.1 Å from the 3'-OH of ωG, suggesting a possible role in leaving group stabilization in the second splicing step (or nucleophile activation in the first step).

The crystal structure of the group I intron derived from bacteriophage *Twort* was solved to 3.6 Å resolution as a complex between the ribozyme and a four-nucleotide product analog (17). Following co-crystallization with Mn^{2+}, a single metal ion within the catalytic site was observed that appeared to correspond to M_A. This metal ion resides within 4 Å of the 3'-OH of U_{-1} and the *pro-S*P nonbridging oxygens of residues U84, A185, and A187 (*Tetrahymena* nucleotides C208, A304, and A306, respectively) (Figure 17). Although the scissile phosphate is absent in this structure, its approximate position could be modeled plausibly so that the *pro-S*P nonbridging oxygen lies within inner sphere coordination distance of the metal ion. A candidate for M_C was not found, but a possible location for such an ion was modeled within 2.5 Å of the ωG 2'-OH and the *pro-S*P nonbridging oxygen of A120 (*Tetrahymena* C262). The *pro-R*P nonbridging oxygen of A187 was also proposed as a ligand for M_C, although subsequent biochemical work has not confirmed this interaction in the *Tetrahymena* ribozyme (111).

The *Tetrahymena* ribozyme itself was solved to 3.8 Å resolution in the absence of substrate (16), after mutations were introduced that improved the thermostability of the ribozyme without significantly affecting catalytic activity (173). Eu^{3+} and Ir^{3+} derivatives revealed a number of metal ion binding sites that were assumed to represent Mg^{2+} sites. Within the catalytic site, one metal ion was found in proximity to both the 2'- and 3'-OH groups of ωG, as well as the nonbridging phosphate oxygens of C262, U305, and A306 (Figure 18). Given this ligand environment, the metal ion was thought to be M_C rather than M_B, despite its apparent contact with the ωG 3'-OH group. The authors noted, however, that the position of this ion would likely shift significantly prior to catalysis due to conformational changes associated with substrate binding. Thus, in the presence of substrate, the ion potentially could become any one of the three catalytic metal ions identified biochemically.

In spite of the overall agreement between the structures and the biochemical data, some discrepancies remain unresolved. The most significant is the lack of any electron density in the structures that might confirm convincingly the presence of M_B. Several possibilities could explain this observation, with the simplest being that M_B does not occupy its binding site in these crystals. This may result from the crystallization conditions themselves. Of the three catalytic metal ions, M_B binds an order of magnitude more weakly than M_A or M_C, and its binding might therefore be more sensitive to variables like ionic strength or the presence of other salts or organic compounds. Alternatively, the ribozymes within the crystals could exist in conformations incompatible with the binding of M_B. Or, M_B could be present in the crystals, but disordered and therefore not visible at the current resolutions.

Other possibilities involve the precise role of M_B in the reaction mechanism. The evidence for the presence of M_B comes from metal ion rescue experiments using a sulfur-modified oligonucleotide substrate in the reverse reaction. Rescue of this particular reaction may require an ion acting as M_B, even though the unmodified forward reaction does not. The ribozymes themselves may even have slightly different reaction mechanisms. The three-metal ion model relies on data obtained from the *Tetrahymena* ribozyme only. This ribozyme may indeed use M_B to effect catalysis, while the *Azoarcus* and *Twort* ribozymes may not. Applying metal ion rescue and TFA techniques to other group I ribozymes should help to address whether a three-metal ion mechanism is unique to *Tetrahymena*.

Metal ion rescue in RNase P

RNase P is an essential endonuclease found in nearly all bacterial, archaeal, and eukaryal organisms (174, 175) (Figure 19). It removes the 5' leader sequence of precursor tRNA molecules (pre-tRNAs) via hydrolysis to produce tRNAs with mature 5' ends. With few exceptions (176), all RNases P are ribonucleoprotein complexes consisting of one or more protein subunits ranging from 120 to 1000 amino acids, combined with a 200- to 400-nucleotide RNA (P RNA). This RNA component contains the catalytic apparatus, as evidenced by the ability of bacterial (177) and some archaeal (178) P RNAs to cleave pre-tRNA *in vitro* in the absence of protein.

The hydrolysis reaction produces a mature tRNA with a 5' phosphate, along with the leader sequence. Catalysis is absolutely dependent on divalent metal ions (179), with a Hill analysis suggesting the involvement of at least three Mg^{2+} ions (180). Site-specific atomic substitutions coupled with metal ion rescue experiments have implicated several ligands on both pre-tRNA and RNase P as important for metal ion binding during catalysis. On the pre-tRNA substrate, phosphorothioate substitution of the *pro-*R_P nonbridging oxygen at the cleavage site reduces the reaction rate by 10^3- to 10^4-fold (132–135, 181). The addition of either Mn^{2+} or Cd^{2+} restores much of this activity (132–135, 182), indicating that the *pro-*R_P nonbridging oxygen coordinates a divalent metal ion during catalysis. This same ion has also been proposed to activate water to generate the hydroxyl nucleophile, based partly on the 6.4-fold rate increase associated with Mn^{2+} rescue of the R_P phosphorothioate reaction (133). In contrast, sulfur substitution of either the *pro-*S_P or the 3' bridging oxygen at the cleavage site shifts cleavage to the next unmodified phosphodiester linkage in the 5' direction (132, 134, 135, 183). The rate of miscleavage is greatly reduced compared with the rate of canonical cleavage in the unmodified reaction. However, softer metal ions have only a minimal effect on the reaction rate and do not change the position of cleavage. This observation suggests that the *pro-*S_P and 3' oxygens at the cleavage site play important roles in catalysis, but whether they coordinate metal ions is unclear. These atoms could be involved in tertiary interactions that the bulkier sulfur atom cannot accommodate. Alternatively, the sulfur atom might exclude catalytic metal ions from the active site, as has been observed for a phosphorothioate substrate bound to the 3'→5' exonuclease site of *E. coli* DNA polymerase I (146, 183).

The 2'-OH group at the cleavage site also appears to coordinate one of the catalytic metal ions. Deoxy substitution of the 2'-OH reduces the reaction rate by 150- to 3400-fold (138, 180, 184). In addition, the Mg^{2+} affinity decreases by four orders of magnitude, with a concomitant reduction in cooperativity from 3 ions to 2 (180). Experiments in which an amino group was installed at the 2' position also suggested a role for the 2'-OH as a metal ion ligand (138). At low pH, substrates bearing a 2'-NH_2 group at the cleavage site showed significant miscleavage in the presence of either Mg^{2+} or Mn^{2+}. Since the 2'-NH_2 group would be protonated at low pH, it would be unable to donate a lone pair of electrons for metal ion coordination. Moreover, the protonated amino group would also repulse any

positively-charged Mg^{2+} ions, further contributing to the loss of cleavage fidelity. At higher pH in the presence of 10 mM Mg^{2+}, the 2'-NH_2 modification resulted in a more than 2500-fold decrease in the reaction rate. While 10 mM Mn^{2+} accelerated the reaction by almost 100-fold, it had a similar effect in the presence of the 2'-H substitution. This result led the authors to propose that the 2'-OH group coordinated a metal ion indirectly through a bound water molecule (outer sphere).

The active site picture that emerges from these experiments is shown in Figure 19B, in which water molecules and functional groups on the pre-tRNA substrate coordinate three metal ions (175). One metal ion binds both the *pro*-R_P nonbridging oxygen and the attacking hydroxyl nucleophile. A second metal ion binds both the *pro*-R_P nonbridging and the 3' bridging oxygens, while a third interacts with the *pro*-S_P nonbridging oxygen and indirectly with the cleavage site 2'-OH group. However, most of these interactions have not yet been confirmed, through either functional experiments or crystallography, to the same extent as those within the *Tetrahymena* active site.

On the P RNA itself, much effort has focused on the P4 helix within the catalytic domain as a candidate site for metal ion coordination (Figure 19D). Phylogenetic analysis has shown that several residues within P4 are highly conserved among bacterial, archaeal, and eukaryal RNase P RNAs (185). In addition, NAIM studies have implicated specific nonbridging oxygens and purine N7 groups within helix P4 as potential ligands (136, 186, 187). In particular, phosphorothioate substitution of either nonbridging oxygen of A67 (*E. coli* numbering) reduces the catalytic rate constant by 10^3- to 10^4-fold (136). Both Mn^{2+} and Cd^{2+} rescue the reactions of the A67-R_P and A67-S_P P RNAs, supporting a role for these nonbridging oxygens in metal ion coordination during catalysis. Similar results were obtained for the homologous position in *B. subtilis* P RNA, although the extent of rescue varied depending on the presence or absence of the P protein (188). Quantitative analysis of Mn^{2+} rescue of the A67-R_P and S_P ribozyme reactions revealed two different affinities for the rescuing Mn^{2+} ion (137). As with the *Tetrahymena* ribozyme (121), this result suggested that two distinct metal ions bound each of the nonbridging oxygens of A67 during catalysis. Experiments using the A67-S_P ribozyme combined with 7-deaza-adenosine substitution of A66 supported a model in which one of these metal ions bound the N7 of A66 and the *pro*-S_P oxygen of A67 simultaneously (137). Evidence for a possible third metal ion binding within the P4 helix came form analagous experiments with 7-deaza-adenosine substitution of A65 (137).

Although these results suggest that the P4 helix binds metal ions important for catalysis, the specific atoms within P4 that coordinate metal ions at the cleavage site are not yet known. A cross-linking study that substituted 4-thiouridine for the conserved bulged uridine U69 demonstrated that the P4 helix does lie in the vicinity of the 5' leader sequence (139). However, the bulge itself, along with other residues postulated to position catalytic metal ions, is situated about 5 nucleotides downstream from the cleavage site, too far to interact with it directly. This result was consistent with models derived from two different crystal structures of bacterial P RNAs (22, 23), which indicated that the P4 metal binding sites were distant from the proposed catalytic center. To determine whether P4 was linked to the catalytic metal ions at the cleavage site, Christian *et al.* mutated the bulged U69 and determined the Cd^{2+} dependence for rescue of an R_P phosphorothioate at the cleavage site (139). Replacing U69 with adenine did not affect the affinity of rescuing Cd^{2+} ions. In contrast, deletion or repositioning of the bulged uridine within the helix resulted in a significant decrease in Cd^{2+} affinity and cooperativity. Substitution of 4-thiouridine for a bulged uridine repositioned at U68 resulted in a cross-link shifted further into the 5' leader sequence relative to the cross-link obtained with unmodified P RNA. Taken together, these observations suggested that the P4 helix positions both the catalytic metal ions and the pre-

tRNA substrate within the active site. As of this writing, however, an atomic model of the RNase P transition state comparable to that deduced for the *Tetrahymena* ribozyme has not been described.

Conclusions

Identifying ligands that bind and position the catalytic metal ions within ribozymes remains an essential prerequisite for the elucidation of ribozyme mechanisms. A plethora of both low and high resolution techniques – biochemical, crystallographic, spectroscopic – have delineated many of the qualitative and quantitative contributions of these interactions to catalysis. As the preceding discussions illustrate, no individual strategy by itself can locate unequivocally all of the metal ions that activate the reacting species and facilitate catalysis. Rather, the most complete picture of metal ion interactions within ribozyme transition states emerges when observations derived from many different approaches are combined and reconciled with each other.

Acknowledgments

The authors would like to thank Mr. Raghuvir Sengupta for his thoughtful advice and comments on the manuscript. J.K.F. is supported by the Medical Scientist Training Program of the University of Chicago Pritzker School of Medicine. J.A.P. is an Investigator in the Howard Hughes Medical Institute.

REFERENCES

1. Herschlag D, Cech TR. Biochemistry. 1990; 29:10159–10171. [PubMed: 2271645]
2. Pyle AM. Science. 1993; 261:709–714. [PubMed: 7688142]
3. Murray JB, Seyhan AA, Walter NG, Burke JM, Scott WG. Chem Biol. 1998; 5:587–595. [PubMed: 9818150]
4. Nakano S, Chadalavada DM, Bevilacqua PC. Science. 2000; 287:1493–1497. [PubMed: 10688799]
5. Perrotta AT, Been MD. Biochemistry. 2006; 45:11357–11365. [PubMed: 16981696]
6. Roth A, Nahvi A, Lee M, Jona I, Breaker RR. RNA. 2006; 12:607–619. [PubMed: 16484375]
7. Sigel RK, Pyle AM. Chem Rev. 2007; 107:97–113. [PubMed: 17212472]
8. Bukhman YV, Draper DE. J Mol Biol. 1997; 273:1020–1031. [PubMed: 9367788]
9. Nakano S, Proctor DJ, Bevilacqua PC. Biochemistry. 2001; 40:12022–12038. [PubMed: 11580278]
10. Nakano S, Cerrone AL, Bevilacqua PC. Biochemistry. 2003; 42:2982–2994. [PubMed: 12627964]
11. Nakano S, Bevilacqua PC. Biochemistry. 2007; 46:3001–3012. [PubMed: 17315949]
12. Ke A, Zhou K, Ding F, Cate JH, Doudna JA. Nature. 2004; 429:201–205. [PubMed: 15141216]
13. Chen JH, Gong B, Bevilacqua PC, Carey PR, Golden BL. Biochemistry. 2009; 48:1498–1507. [PubMed: 19178151]
14. Williams LD. Top Curr Chem. 2005; 253:77–88.
15. Adams PL, Stahley MR, Kosek AB, Wang J, Strobel SA. Nature. 2004; 430:45–50. [PubMed: 15175762]
16. Guo F, Gooding AR, Cech TR. Mol Cell. 2004; 16:351–362. [PubMed: 15525509]
17. Golden BL, Kim H, Chase E. Nat Struct Mol Biol. 2005; 12:82–89. [PubMed: 15580277]
18. Stahley MR, Strobel SA. Science. 2005; 309:1587–1590. [PubMed: 16141079]
19. Toor N, Keating KS, Taylor SD, Pyle AM. Science. 2008; 320:77–82. [PubMed: 18388288]
20. Toor N, Rajashankar K, Keating KS, Pyle AM. Nat Struct Mol Biol. 2008; 15:1221–1222. [PubMed: 18953333]
21. Krasilnikov AS, Yang X, Pan T, Mondragon A. Nature. 2003; 421:760–764. [PubMed: 12610630]
22. Kazantsev AV, Krivenko AA, Harrington DJ, Holbrook SR, Adams PD, Pace NR. Proc Natl Acad Sci USA. 2005; 102:13392–13397. [PubMed: 16157868]

23. Torres-Larios A, Swinger KK, Krasilnikov AS, Pan T, Mondragon A. Nature. 2005; 437:584–587. [PubMed: 16113684]
24. Ban N, Nissen P, Hansen J, Moore PB, Steitz TA. Science. 2000; 289:905–920. [PubMed: 10937989]
25. Wimberly BT, Brodersen DE, Clemons WM Jr, Morgan-Warren RJ, Carter AP, Vonrhein C, Hartsch T, Ramakrishnan V. Nature. 2000; 407:327–339. [PubMed: 11014182]
26. Clemons WM Jr, Brodersen DE, McCutcheon JP, May JL, Carter AP, Morgan-Warren RJ, Wimberly BT, Ramakrishnan V. J Mol Biol. 2001; 310:827–843. [PubMed: 11453691]
27. Pley HW, Lindes DS, DeLuca-Flaherty C, McKay DB. J Biol Chem. 1993; 268:19656–19658. [PubMed: 8366108]
28. Pley HW, Flaherty KM, McKay DB. Nature. 1994; 372:68–74. [PubMed: 7969422]
29. Scott, WG.; Finch, JT.; Klug, A. Nucleic Acids Symp Ser; 1995. p. 214-216.
30. Scott WG, Murray JB, Arnold JR, Stoddard BL, Klug A. Science. 1996; 274:2065–2069. [PubMed: 8953035]
31. Martick M, Scott WG. Cell. 2006; 126:309–320. [PubMed: 16859740]
32. Rupert PB, Ferre-D'Amare AR. Nature. 2001; 410:780–786. [PubMed: 11298439]
33. Rupert PB, Massey AP, Sigurdsson ST, Ferre-D'Amare AR. Science. 2002; 298:1421–1424. [PubMed: 12376595]
34. Ferre-D'Amare AR, Zhou K, Doudna JA. Nature. 1998; 395:567–574. [PubMed: 9783582]
35. Ferre-D'Amare AR, Doudna JA. J Mol Biol. 2000; 295:541–556. [PubMed: 10623545]
36. Klein DJ, Ferre-D'Amare AR. Science. 2006; 313:1752–1756. [PubMed: 16990543]
37. Ye JD, Tereshko V, Frederiksen JK, Koide A, Fellouse FA, Sidhu SS, Koide S, Kossiakoff AA, Piccirilli JA. Proc Natl Acad Sci USA. 2008; 105:82–87. [PubMed: 18162543]
38. Kovall RA, Matthews BW. Curr Opin Chem Biol. 1999; 3:578–583. [PubMed: 10508668]
39. Pingoud A, Jeltsch A. Nucleic Acids Res. 2001; 29:3705–3727. [PubMed: 11557805]
40. Galburt EA, Stoddard BL. Biochemistry. 2002; 41:13851–13860. [PubMed: 12437341]
41. Nelson JA, Uhlenbeck OC. Mol Cell. 2006; 23:447–450. [PubMed: 16916633]
42. DeRose, VJ. Nucleic Acid-Metal Ion Interactions. Hud, NV., editor. Cambridge, UK: Royal Society of Chemistry; 2009. p. 154-179.
43. Horton TE, Clardy DR, DeRose VJ. Biochemistry. 1998; 37:18094–18101. [PubMed: 9922178]
44. Morrissey SR, Horton TE, DeRose VJ. J Am Chem Soc. 2000; 122:3473–3481.
45. Kisseleva N, Khvorova A, Westhof E, Schiemann O. RNA. 2005; 11:1–6. [PubMed: 15611296]
46. Vogt M, Lahiri S, Hoogstraten CG, Britt RD, DeRose VJ. J Am Chem Soc. 2006; 128:16764–16770. [PubMed: 17177426]
47. Salemink PJ, Swarthof T, Hilbers CW. Biochemistry. 1979; 18:3477–3485. [PubMed: 383144]
48. Hilbers CW, Heerschap A, Haasnoot CA, Walters JA. J Biomol Struct Dyn. 1983; 1:183–207. [PubMed: 6401111]
49. Cheong C, Varani G, Tinoco I Jr. Nature. 1990; 346:680–682. [PubMed: 1696688]
50. Dieckmann T, Suzuki E, Nakamura GK, Feigon J. RNA. 1996; 2:628–640. [PubMed: 8756406]
51. Butcher SE, Dieckmann T, Feigon J. EMBO J. 1997; 16:7490–7499. [PubMed: 9405377]
52. Sashital DG, Venditti V, Angers CG, Cornilescu G, Butcher SE. RNA. 2007; 13:328–338. [PubMed: 17242306]
53. Wu M, Tinoco I Jr. Proc Natl Acad Sci USA. 1998; 95:11555–11560. [PubMed: 9751704]
54. Al-Hashimi HM, Pitt SW, Majumdar A, Xu W, Patel DJ. J Mol Biol. 2003; 329:867–873. [PubMed: 12798678]
55. Maderia M, Hunsicker LM, DeRose VJ. Biochemistry. 2000; 39:12113–12120. [PubMed: 11015188]
56. Butcher SE, Allain FH, Feigon J. Biochemistry. 2000; 39:2174–2182. [PubMed: 10694382]
57. Noeske J, Schwalbe H, Wohnert J. Nucleic Acids Res. 2007; 35:5262–5273. [PubMed: 17686787]
58. Reid SS, Cowan JA. Biochemistry. 1990; 29:6025–6032. [PubMed: 2383570]
59. Grant CV, Frydman V, Frydman L. J Am Chem Soc. 2000; 122:11743–11744.

60. Grant CV, Frydman V, Harwood JS, Frydman L. J Am Chem Soc. 2002; 124:4458–4462. [PubMed: 11960475]
61. Marincola FC, Casu M, Saba G, Manetti C, Lai A. Phys Chem Chem Phys. 2000; 2:2425–2428.
62. Denisov VP, Halle B. Proc Natl Acad Sci USA. 2000; 97:629–633. [PubMed: 10639130]
63. Marincola FC, Denisov VP, Halle B. J Am Chem Soc. 2004; 126:6739–6750. [PubMed: 15161302]
64. Gill ML, Strobel SA, Loria JP. J Am Chem Soc. 2005; 127:16723–16732. [PubMed: 16305263]
65. Hunsicker-Wang, LM. Ph.D. Thesis. Texas A&M University; 2001.
66. Kayne MS, Cohn M. Biochemistry. 1974; 13:4159–4165. [PubMed: 4606518]
67. Draper DE. Biophys Chem. 1985; 21:91–101. [PubMed: 3978219]
68. Greenbaum NL, Mundoma C, Peterman DR. Biochemistry. 2001; 40:1124–1134. [PubMed: 11170437]
69. Yuan F, Griffin L, Phelps L, Buschmann V, Weston K, Greenbaum NL. Nucleic Acids Res. 2007; 35:2833–2845. [PubMed: 17430967]
70. Feig AL, Panek M, Horrocks WD Jr, Uhlenbeck OC. Chem Biol. 1999; 6:801–810. [PubMed: 10574781]
71. Walter NG, Yang N, Burke JM. J Mol Biol. 2000; 298:539–555. [PubMed: 10772868]
72. Tinsley RA, Walter NG. Biol Chem. 2007; 388:705–715. [PubMed: 17570823]
73. Gong B, Chen Y, Christian EL, Chen JH, Chase E, Chadalavada DM, Yajima R, Golden BL, Bevilacqua PC, Carey PR. J Am Chem Soc. 2008; 130:9670–9672. [PubMed: 18593125]
74. Chin K, Sharp KA, Honig B, Pyle AM. Nat Struct Biol. 1999; 6:1055–1061. [PubMed: 10542099]
75. Hermann T, Westhof E. Structure. 1998; 6:1303–1314. [PubMed: 9782053]
76. Bagley SC, Altman RB. Protein Sci. 1995; 4:622–635. [PubMed: 7613462]
77. Banatao DR, Altman RB, Klein TE. Nucleic Acids Res. 2003; 31:4450–4460. [PubMed: 12888505]
78. Castagnetto JM, Hennessy SW, Roberts VA, Getzoff ED, Tainer JA, Pique ME. Nucleic Acids Res. 2002; 30:379–382. [PubMed: 11752342]
79. Stefan LR, Zhang R, Levitan AG, Hendrix DK, Brenner SE, Holbrook SR. Nucleic Acids Res. 2006; 34:D131–D134. [PubMed: 16381830]
80. Klosterman PS, Tamura M, Holbrook SR, Brenner SE. Nucleic Acids Res. 2002; 30:392–394. [PubMed: 11752346]
81. Sigel RK, Vaidya A, Pyle AM. Nat Struct Biol. 2000; 7:1111–1116. [PubMed: 11101891]
82. Kaye NM, Zahler NH, Christian EL, Harris ME. J Mol Biol. 2002; 324:429–442. [PubMed: 12445779]
83. Harris DA, Tinsley RA, Walter NG. J Mol Biol. 2004; 341:389–403. [PubMed: 15276831]
84. Hargittai MR, Musier-Forsyth K. RNA. 2000; 6:1672–1680. [PubMed: 11105765]
85. Harris DA, Walter NG. Curr Protoc Nucleic Acid Chem. 2003; Chapter 6(Unit 6.8)
86. Harris ME, Cassano AG. Curr Opin Chem Biol. 2008; 12:626–639. [PubMed: 18952193]
87. Buddenbaum WE, Shiner VJ. Can J Chem. 1976; 54:1146–1161.
88. Paneth P, Oleary MH. J Am Chem Soc. 1991; 113:1691–1693.
89. Hengge AC, Sowa GA, Wu L, Zhang ZY. Biochemistry. 1995; 34:13982–13987. [PubMed: 7577995]
90. Hengge AC, Bruzik KS, Tobin AE, Cleland WW, Tsai MD. Bioorg Chem. 2000; 28:119–133. [PubMed: 10915550]
91. Gerratana B, Sowa GA, Cleland WW. J Am Chem Soc. 2000; 122:12615–12621.
92. Cassano AG, Anderson VE, Harris ME. J Am Chem Soc. 2002; 124:10964–10965. [PubMed: 12224928]
93. Shih IH, Been MD. Proc Natl Acad Sci USA. 2001; 98:1489–1494. [PubMed: 11171978]
94. Smith MD, Collins RA. Proc Natl Acad Sci USA. 2007; 104:5818–5823. [PubMed: 17389378]
95. Rishavy MA, Hengge AC, Cleland WW. Bioorg Chem. 2000; 28:283–292. [PubMed: 11133147]

96. Humphry T, Forconi M, Williams NH, Hengge AC. J Am Chem Soc. 2002; 124:14860–14861. [PubMed: 12475323]
97. Rawlings J, Cleland WW, Hengge AC. J Inorg Biochem. 2003; 93:61–65. [PubMed: 12538053]
98. Humphry T, Forconi M, Williams NH, Hengge AC. J Am Chem Soc. 2004; 126:11864–11869. [PubMed: 15382921]
99. Yang MY, Iranzo O, Richard JP, Morrow JR. J Am Chem Soc. 2005; 127:1064–1065. [PubMed: 15669821]
100. Rawlings J, Cleland WW, Hengge AC. J Am Chem Soc. 2006; 128:17120–17125. [PubMed: 17177465]
101. Cassano AG, Anderson VE, Harris ME. Biochemistry. 2004; 43:10547–10559. [PubMed: 15301552]
102. Cassano AG, Anderson VE, Harris ME. Biopolymers. 2004; 73:110–129. [PubMed: 14691944]
103. Dai Q, Frederiksen JK, Anderson VE, Harris ME, Piccirilli JA. J Org Chem. 2008; 73:309–311. [PubMed: 18052189]
104. Zhong M, Strobel SA. J Org Chem. 2008; 73:603–611. [PubMed: 18081346]
105. Ryder SP, Strobel SA. Methods. 1999; 18:38–50. [PubMed: 10208815]
106. Freisinger E, Sigel RKO. Coord Chem Rev. 2007; 251:1834–1851.
107. Klein DJ, Moore PB, Steitz TA. RNA. 2004; 10:1366–1379. [PubMed: 15317974]
108. Christian EL, Yarus M. Biochemistry. 1993; 32:4475–4480. [PubMed: 7683490]
109. Szewczak AA, Kosek AB, Piccirilli JA, Strobel SA. Biochemistry. 2002; 41:2516–2525. [PubMed: 11851398]
110. Hougland JL, Kravchuk AV, Herschlag D, Piccirilli JA. PLoS Biol. 2005; 3:e277. [PubMed: 16092891]
111. Forconi M, Lee J, Lee JK, Piccirilli JA, Herschlag D. Biochemistry. 2008; 47:6883–6894. [PubMed: 18517225]
112. Sarnovsky RJ, May EW, Craig NL. Embo J. 1996; 15:6348–6361. [PubMed: 8947057]
113. Allingham JS, Pribil PA, Haniford DB. J Mol Biol. 1999; 289:1195–1206. [PubMed: 10373361]
114. Kim DR, Dai Y, Mundy CL, Yang W, Oettinger MA. Genes Dev. 1999; 13:3070–3380. [PubMed: 10601033]
115. Landree MA, Wibbenmeyer JA, Roth DB. Genes Dev. 1999; 13:3059–3069. [PubMed: 10601032]
116. Gao K, Wong S, Bushman F. J Virol. 2004; 78:6715–6722. [PubMed: 15194746]
117. Schwarzer D, Cole PA. Curr Opin Chem Biol. 2005; 9:561–569. [PubMed: 16226484]
118. Piccirilli JA, Vyle JS, Caruthers MH, Cech TR. Nature. 1993; 361:85–88. [PubMed: 8421499]
119. Sjögren AS, Pettersson E, Sjöberg BM, Strömberg R. Nucleic Acids Res. 1997; 25:648–653. [PubMed: 9016608]
120. Weinstein LB, Jones BC, Cosstick R, Cech TR. Nature. 1997; 388:805–808. [PubMed: 9285596]
121. Shan S, Yoshida A, Sun S, Piccirilli JA, Herschlag D. Proc Natl Acad Sci USA. 1999; 96:12299–12304. [PubMed: 10535916]
122. Shan SO, Herschlag D. Biochemistry. 1999; 38:10958–10975. [PubMed: 10460151]
123. Yoshida A, Sun S, Piccirilli JA. Nat Struct Biol. 1999; 6:318–321. [PubMed: 10201397]
124. Shan S, Kravchuk AV, Piccirilli JA, Herschlag D. Biochemistry. 2001; 40:5161–5171. [PubMed: 11318638]
125. Sontheimer EJ, Gordon PM, Piccirilli JA. Genes Dev. 1999; 13:1729–1741. [PubMed: 10398685]
126. Gordon PM, Sontheimer EJ, Piccirilli JA. Biochemistry. 2000; 39:12939–12952. [PubMed: 11041859]
127. Gordon PM, Piccirilli JA. Nat Struct Biol. 2001; 8:893–898. [PubMed: 11573097]
128. Gordon PM, Fong R, Piccirilli JA. Chem Biol. 2007; 14:607–612. [PubMed: 17584608]
129. Peracchi A, Beigelman L, Scott EC, Uhlenbeck OC, Herschlag D. J Biol Chem. 1997; 272:26822–26826. [PubMed: 9341112]

130. Wang S, Karbstein K, Peracchi A, Beigelman L, Herschlag D. Biochemistry. 1999; 38:14363–14378. [PubMed: 10572011]
131. Osborne EM, Schaak JE, DeRose VJ. RNA. 2005; 11:187–196. [PubMed: 15659358]
132. Warnecke JM, Furste JP, Hardt WD, Erdmann VA, Hartmann RK. Proc Natl Acad Sci USA. 1996; 93:8924–8928. [PubMed: 8799129]
133. Chen Y, Li X, Gegenheimer P. Biochemistry. 1997; 36:2425–2438. [PubMed: 9054547]
134. Warnecke JM, Held R, Busch S, Hartmann RK. J Mol Biol. 1999; 290:433–445. [PubMed: 10390342]
135. Pfeiffer T, Tekos A, Warnecke JM, Drainas D, Engelke DR, Seraphin B, Hartmann RK. J Mol Biol. 2000; 298:559–565. [PubMed: 10788319]
136. Christian EL, Kaye NM, Harris ME. RNA. 2000; 6:511–519. [PubMed: 10786842]
137. Christian EL, Kaye NM, Harris ME. EMBO J. 2002; 21:2253–2262. [PubMed: 11980722]
138. Persson T, Cuzic S, Hartmann RK. J Biol Chem. 2003; 278:43394–43401. [PubMed: 12904300]
139. Christian EL, Smith KM, Perera N, Harris ME. RNA. 2006; 12:1463–1467. [PubMed: 16822954]
140. Sontheimer EJ, Sun S, Piccirilli JA. Nature. 1997; 388:801–805. [PubMed: 9285595]
141. Gordon PM, Sontheimer EJ, Piccirilli JA. RNA. 2000; 6:199–205. [PubMed: 10688359]
142. Yean SL, Wuenschell G, Termini J, Lin RJ. Nature. 2000; 408:881–884. [PubMed: 11130730]
143. Pecoraro VL, Hermes JD, Cleland WW. Biochemistry. 1984; 23:5262–5271. [PubMed: 6334536]
144. Frey PA, Sammons RD. Science. 1985; 228:541–545. [PubMed: 2984773]
145. Rablen PR, Lockman JW, Jorgensen WL. J Phys Chem A. 1998; 102:3782–3797.
146. Brautigam CA, Steitz TA. J Mol Biol. 1998; 277:363–377. [PubMed: 9514742]
147. Kruger K, Grabowski PJ, Zaug AJ, Sands J, Gottschling DE, Cech TR. Cell. 1982; 31:147–157. [PubMed: 6297745]
148. Zaug AJ, Been MD, Cech TR. Nature. 1986; 324:429–433. [PubMed: 3537808]
149. Grosshans CA, Cech TR. Biochemistry. 1989; 28:6888–6894. [PubMed: 2684268]
150. Bevilacqua PC, Kierzek R, Johnson KA, Turner DH. Science. 1992; 258:1355–1358. [PubMed: 1455230]
151. Herschlag D. Biochemistry. 1992; 31:1386–1399. [PubMed: 1736996]
152. Herschlag D, Khosla M. Biochemistry. 1994; 33:5291–5297. [PubMed: 8172903]
153. Cosstick R, Vyle JS. Nucleic Acids Res. 1990; 18:829–835. [PubMed: 2315041]
154. Vyle JS, Connolly BA, Kemp D, Cosstick R. Biochemistry. 1992; 31:3012–3018. [PubMed: 1550825]
155. Herschlag D, Cech TR. Nature. 1990; 344:405–409. [PubMed: 1690858]
156. Shan SO, Herschlag D. RNA. 2000; 6:795–813. [PubMed: 10864040]
157. Steitz TA, Steitz JA. Proc Natl Acad Sci USA. 1993; 90:6498–6502. [PubMed: 8341661]
158. Freemont PS, Friedman JM, Beese LS, Sanderson MR, Steitz TA. Proc Natl Acad Sci USA. 1988; 85:8924–8928. [PubMed: 3194400]
159. Beese LS, Steitz TA. Embo J. 1991; 10:25–33. [PubMed: 1989886]
160. Kim EE, Wyckoff HW. J Mol Biol. 1991; 218:449–464. [PubMed: 2010919]
161. Dantzman CL, Kiessling LL. J Am Chem Soc. 1996; 118:11715–11719.
162. Bass BL, Cech TR. Nature. 1984; 308:820–826. [PubMed: 6562377]
163. McConnell TS, Cech TR. Biochemistry. 1995; 34:4056–4067. [PubMed: 7696271]
164. Gott JM, Shub DA, Belfort M. Cell. 1986; 47:81–87. [PubMed: 3757035]
165. Stromberg R, Hahne S, Sjogren AS, Sjoberg BM. Biochem Biophys Res Commun. 1992; 183:842–848. [PubMed: 1550590]
166. Shan SO, Herschlag D. RNA. 2002; 8:861–872. [PubMed: 12166641]
167. Herschlag D, Piccirilli JA, Cech TR. Biochemistry. 1991; 30:4844–4854. [PubMed: 2036355]
168. Michel F, Westhof E. J Mol Biol. 1990; 216:585–610. [PubMed: 2258934]
169. Ortoleva-Donnelly L, Szewczak AA, Gutell RR, Strobel SA. RNA. 1998; 4:498–519. [PubMed: 9582093]

170. Strauss-Soukup JK, Strobel SA. J Mol Biol. 2000; 302:339–358. [PubMed: 10970738]
171. Moore MJ, Sharp PA. Science. 1992; 256:992–997. [PubMed: 1589782]
172. Forconi M, Lee J, Hougland JL, Piccirilli JA, Herschlag D. unpublished.
173. Guo F, Cech TR. Nat Struct Biol. 2002; 9:855–861. [PubMed: 12368901]
174. Evans D, Marquez SM, Pace NR. Trends Biochem Sci. 2006; 31:333–341. [PubMed: 16679018]
175. Kazantsev AV, Pace NR. Nat Rev Microbiol. 2006; 4:729–740. [PubMed: 16980936]
176. Wang MJ, Davis NW, Gegenheimer P. EMBO J. 1988; 7:1567–1574. [PubMed: 16453848]
177. Guerrier-Takada C, Gardiner K, Marsh T, Pace N, Altman S. Cell. 1983; 35:849–857. [PubMed: 6197186]
178. Pannucci JA, Haas ES, Hall TA, Harris JK, Brown JW. Proc Natl Acad Sci USA. 1999; 96:7803–7808. [PubMed: 10393902]
179. Beebe JA, Kurz JC, Fierke CA. Biochemistry. 1996; 35:10493–10505. [PubMed: 8756706]
180. Smith D, Pace NR. Biochemistry. 1993; 32:5273–5281. [PubMed: 8499432]
181. Kahle D, Kust B, Krupp G. Biochimie. 1993; 75:955–962. [PubMed: 8123702]
182. Warnecke JM, Green CJ, Hartmann RK. Nucleosides & Nucleotides. 1997; 16:721–725.
183. Warnecke JM, Sontheimer EJ, Piccirilli JA, Hartmann RK. Nucleic Acids Res. 2000; 28:720–727. [PubMed: 10637323]
184. Loria A, Pan T. Biochemistry. 1998; 37:10126–10133. [PubMed: 9665718]
185. Chen JL, Pace NR. RNA. 1997; 3:557–560. [PubMed: 9174091]
186. Harris ME, Pace NR. RNA. 1995; 1:210–218. [PubMed: 7585250]
187. Kaye NM, Christian EL, Harris ME. Biochemistry. 2002; 41:4533–4545. [PubMed: 11926814]
188. Crary SM, Kurz JC, Fierke CA. RNA. 2002; 8:933–947. [PubMed: 12166648]

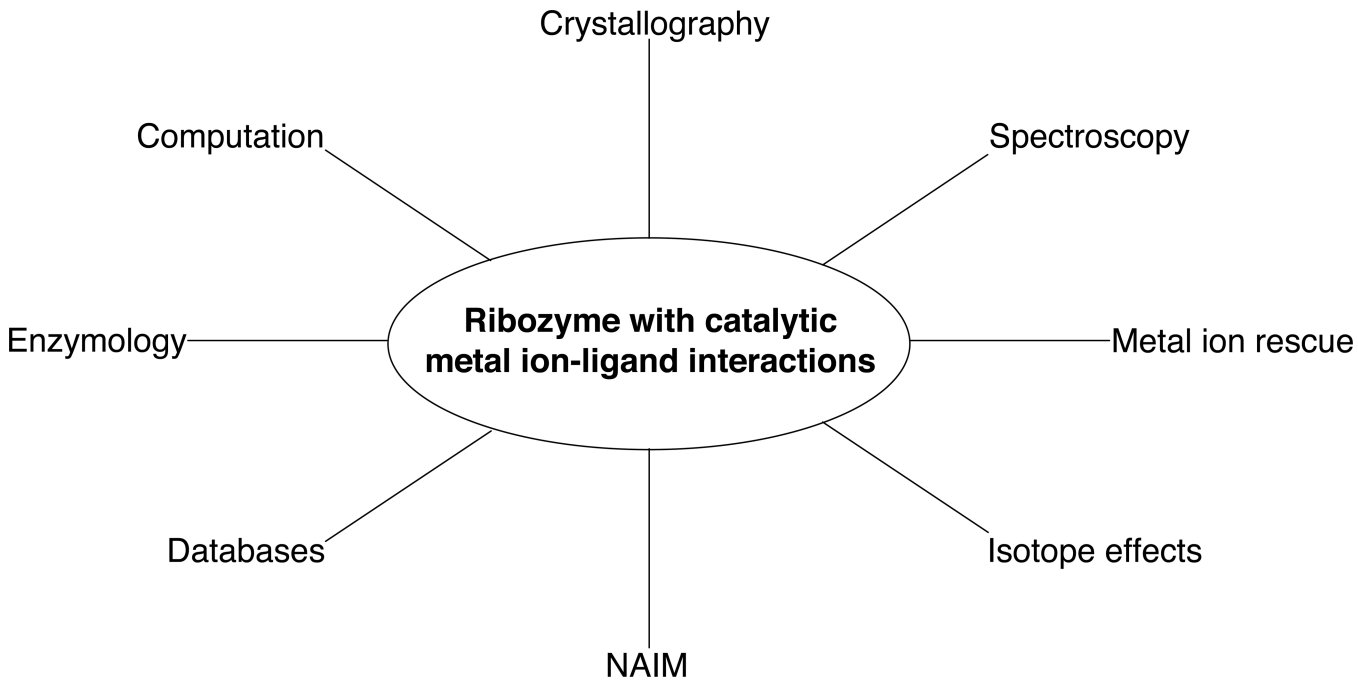

Figure 1.
Summary of techniques used to identify catalytic metal ion-ligand interactions within ribozymes.

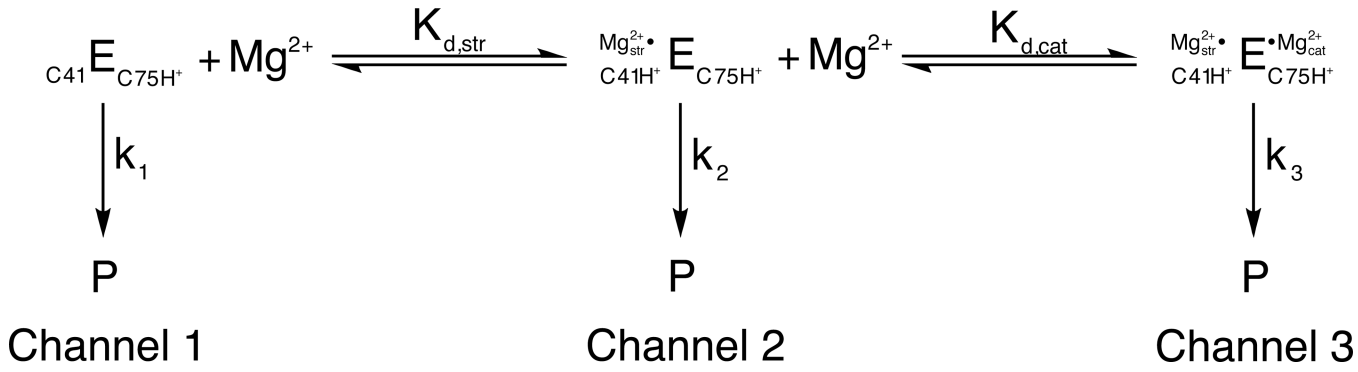

Figure 2.

A three-channel scheme describing the Mg^{2+}-dependent and independent pathways for HDV ribozyme catalysis. In 1 M NaCl in the absence of Mg^{2+}, the ribozyme reacts at a basal rate with rate constant k_1 (channel 1). Increasing concentrations of Mg^{2+} accelerate this rate in a log-linear fashion (channel 2) up to a point, after which the rate becomes independent of Mg^{2+} concentration (channel 3). The Mg^{2+} ion associated with channel 2 conditions is thought to be primarily structural, binding via inner sphere coordination to a base quadruple involving a protonated C41. Under channel 3 conditions, a second, catalytic, Mg^{2+} ion binds via outer sphere coordination in the vicinity of the active site. This fully hydrated Mg^{2+} ion is thought to participate in general acid-base catalysis. [Adapted from (10).]

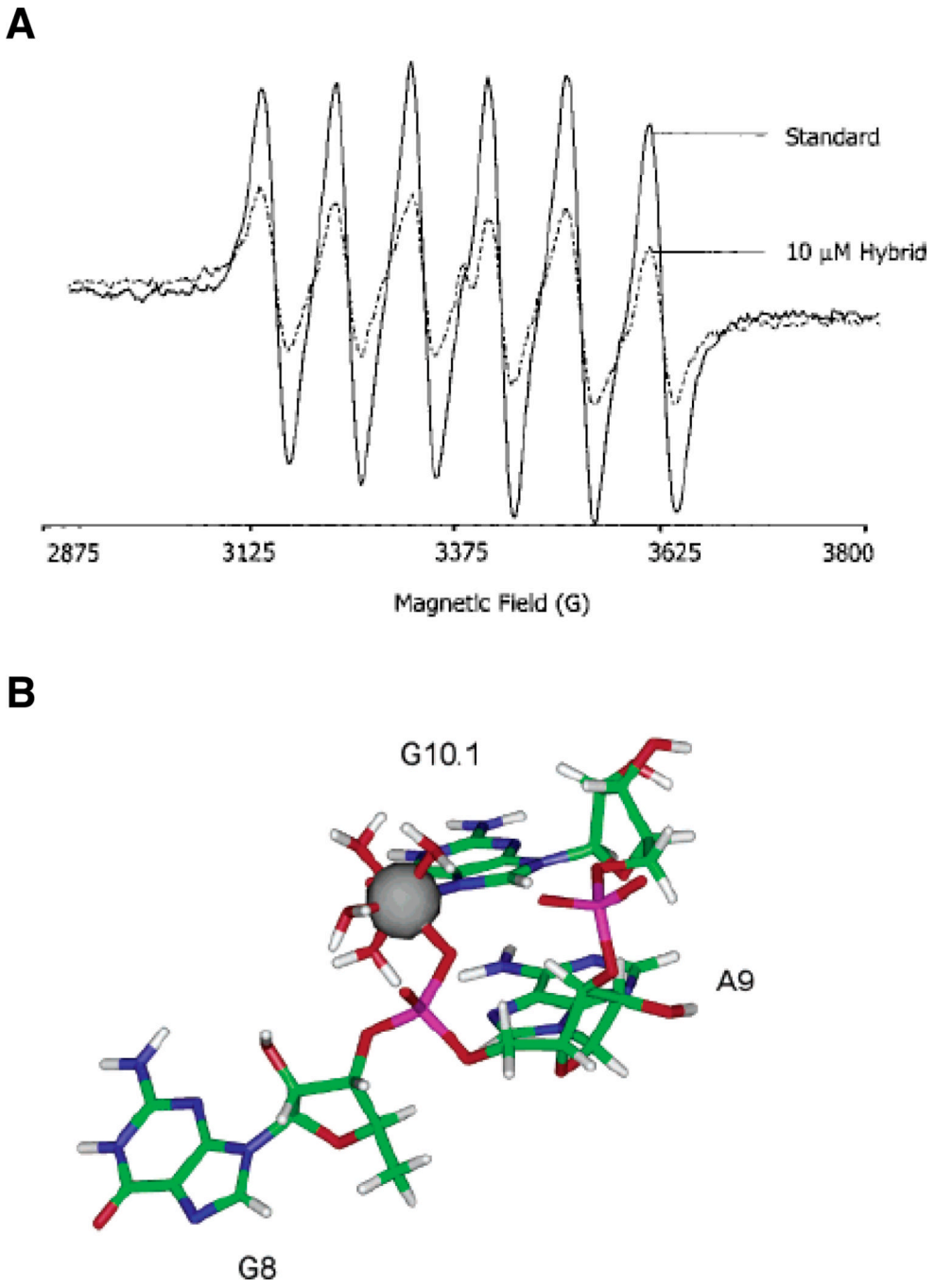

Figure 3.

EPR spectroscopy of a Mn^{2+} binding site within the hammerhead ribozyme. (A) EPR spectra of a 50 μM solution of Mn^{2+} alone (solid line) and in the presence of 10 μM of an RNA-DNA hybrid hammerhead ribozyme (dotted line). The addition of nucleic acid causes the six-line EPR spectrum of Mn^{2+} to diminish. (B) Model of the A9/G10.1 Mn^{2+} binding site in the tertiary-stabilized hammerhead ribozyme, as determined through energy minimization of crystallographic and ESEEM data. The Mn^{2+} ion coordinates the *pro-*R_P nonbridging oxygen of A9, the N7 of G10.1, and four water molecules. [Taken from (43) and (46), with permission.]

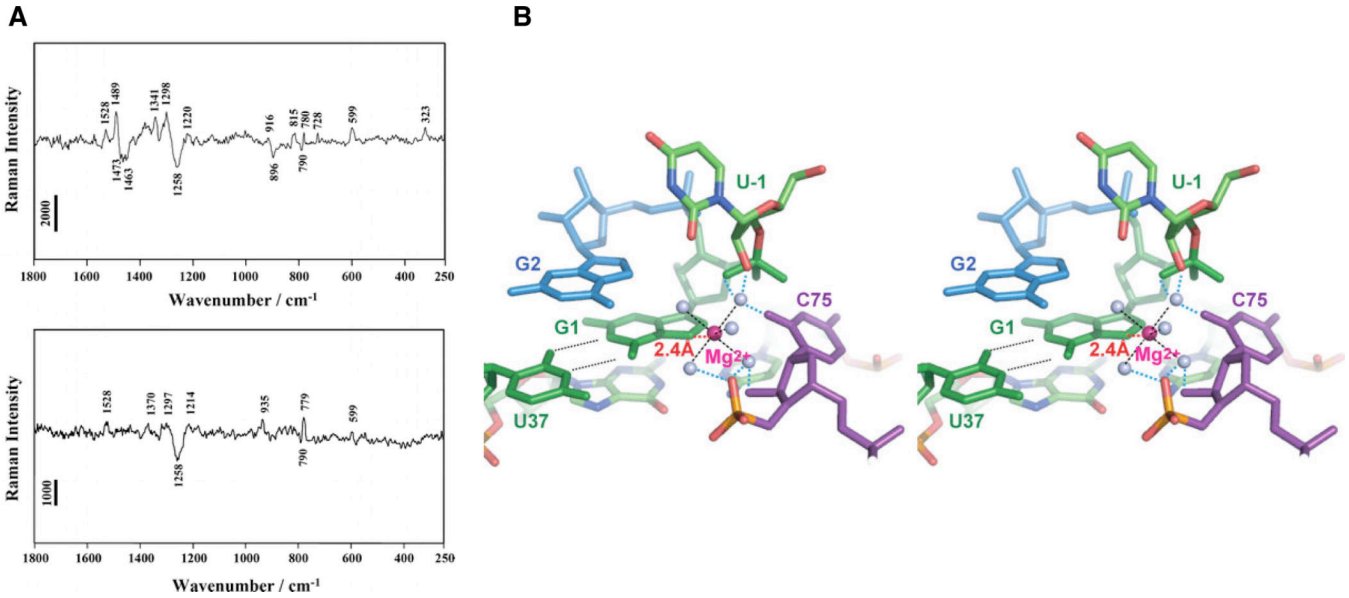

Figure 4.

Raman spectroscopic investigation of HDV ribozyme crystals. (A) Raman difference spectra (pH 7.5 – pH 5.0) of crystals of the unmodified HDV ribozyme (top panel) and an HDV ribozyme in which 7-deazaguanosine has replaced the cleavage site G1 (bottom panel). The difference spectrum of the unmodified ribozyme shows peaks at 1489 and 323 cm^{-1}, thought to arise from metal ion coordination of a guanosine N7 and from a single inner sphere Mg^{2+} hydrate, respectively. Both features are lost when 7-deazaguanosine replaces guanosine at the cleavage site. (B) Stereo model of the HDV ribozyme active site, constructed by combining the Raman spectroscopic results with pre- and post-cleavage crystallographic data. The Mg^{2+} ion (magenta) directly coordinates the N7 of G1, along with five water molecules (grey spheres). [Taken from (13), with permission.]

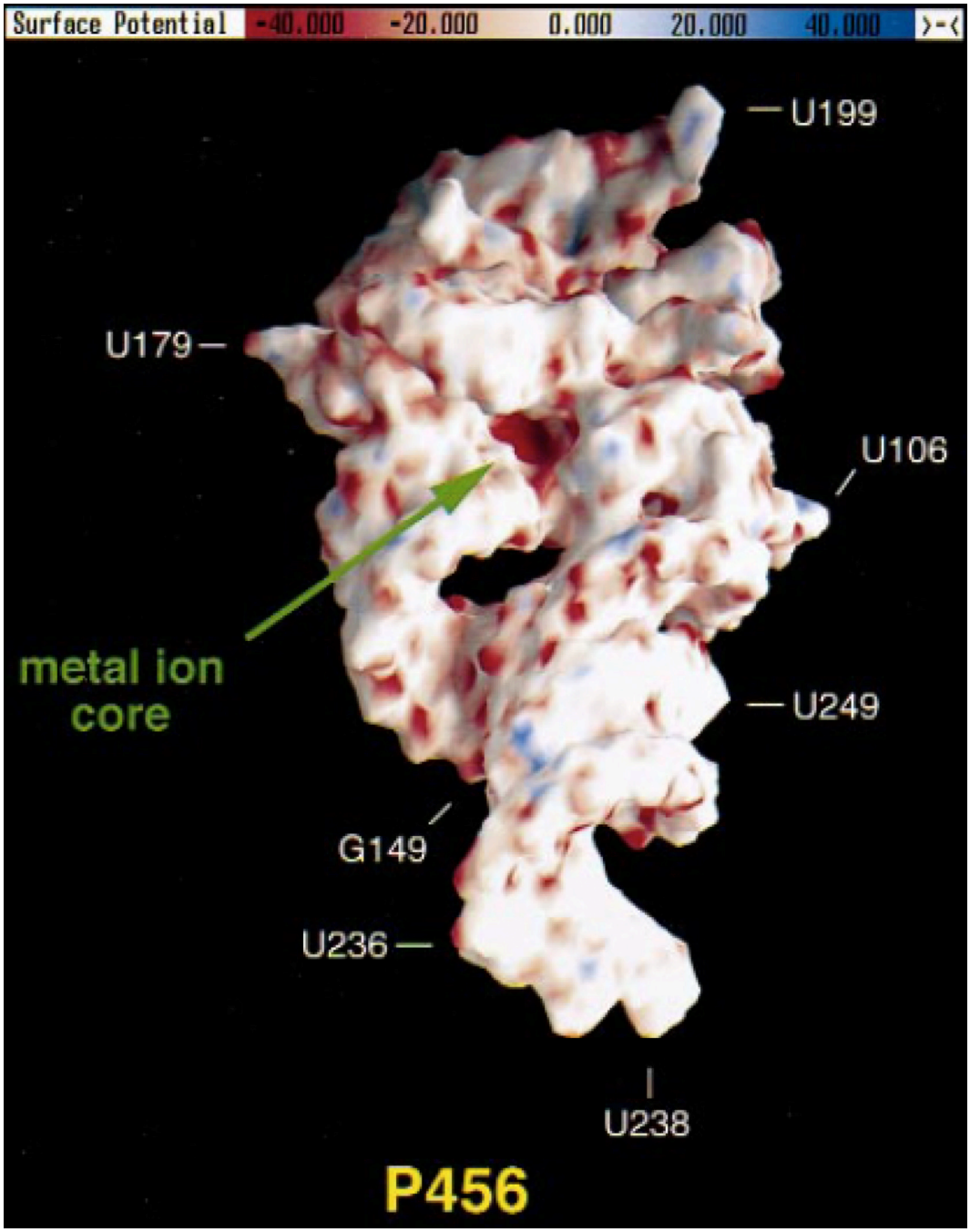

Figure 5.
Electrostatic potential surface of the P4–P6 domain from the *Tetrahymena* group I ribozyme, calculated using the NLPB equation. Regions of negative electrostatic potential appear red, while electropositive regions appear blue. The A-rich bulge that coordinates two Mg^{2+} ions is located in a pocket of highly negative electrostatic potential ("metal ion core") with values ranging from −80 to −100 kT/e. [Adapted from (74), with permission.]

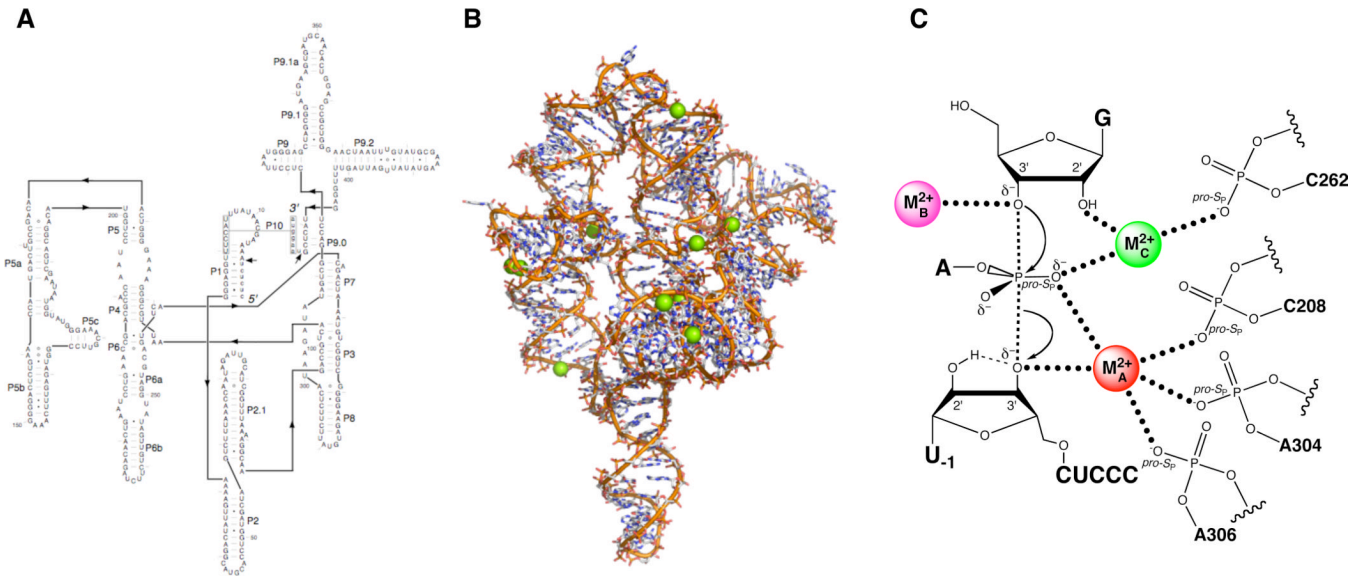

Figure 6.

The *Tetrahymena* group I ribozyme. (A) Secondary structure. (B) Three-dimensional structure at 3.8 Å resolution (PDB file 1X8W). Mg^{2+} ions are represented as green spheres. (C) Transition state catalytic metal ion-ligand interactions within the *Tetrahymena* ribozyme active site, as deduced from metal ion rescue experiments.

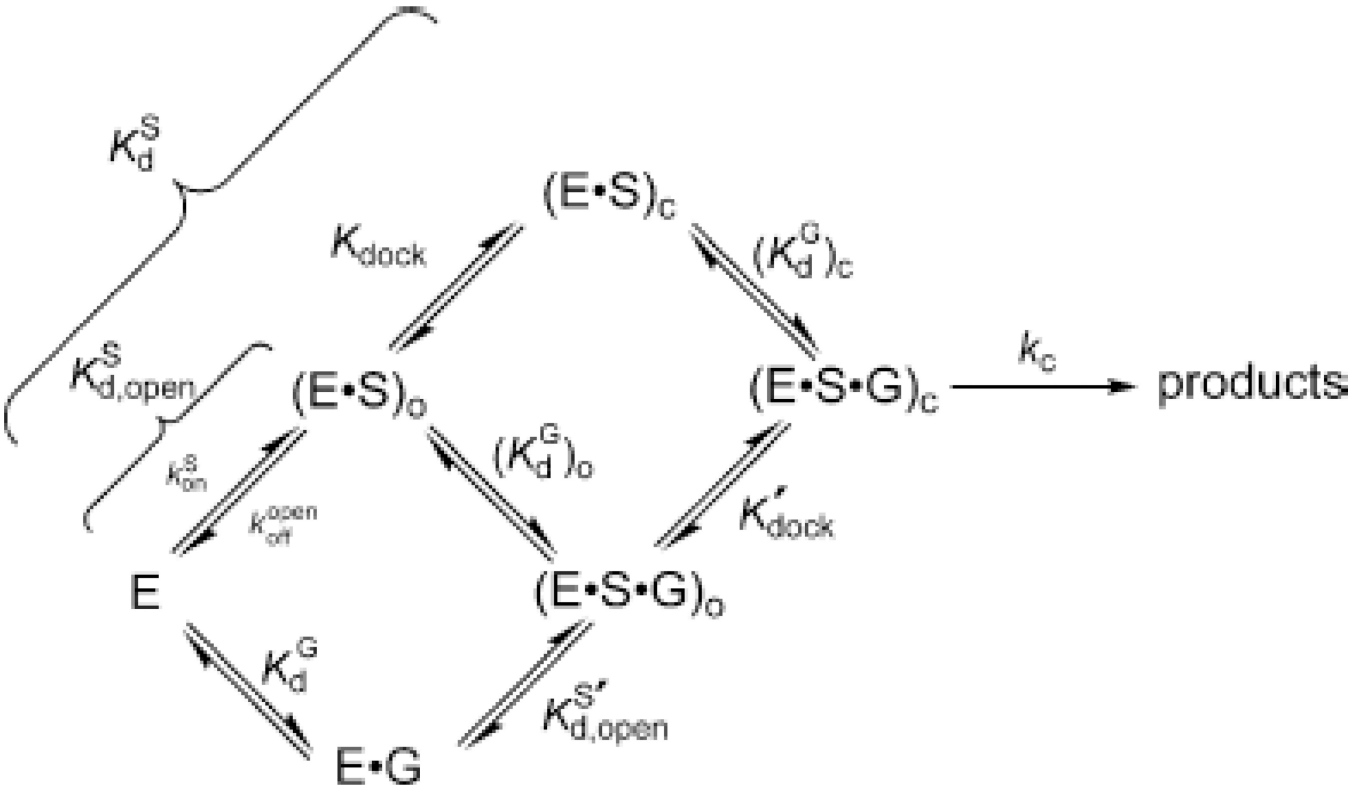

Figure 7.

Kinetic model of the *Tetrahymena* ribozyme reaction. The free enzyme (E) can bind the oligonucleotide substrate (S) to form the open complex, in the presence $[(E{\cdot}S{\cdot}G)_O]$ or absence $[(E{\cdot}S)_O]$ of guanosine. The closed complex $[(E{\cdot}S{\cdot}G)_C$ or $(E{\cdot}S)_C]$ forms when the P1 helix carrying the substrate "docks" into the active site of the ribozyme via the formation of tertiary interactions. [Taken from (111).]

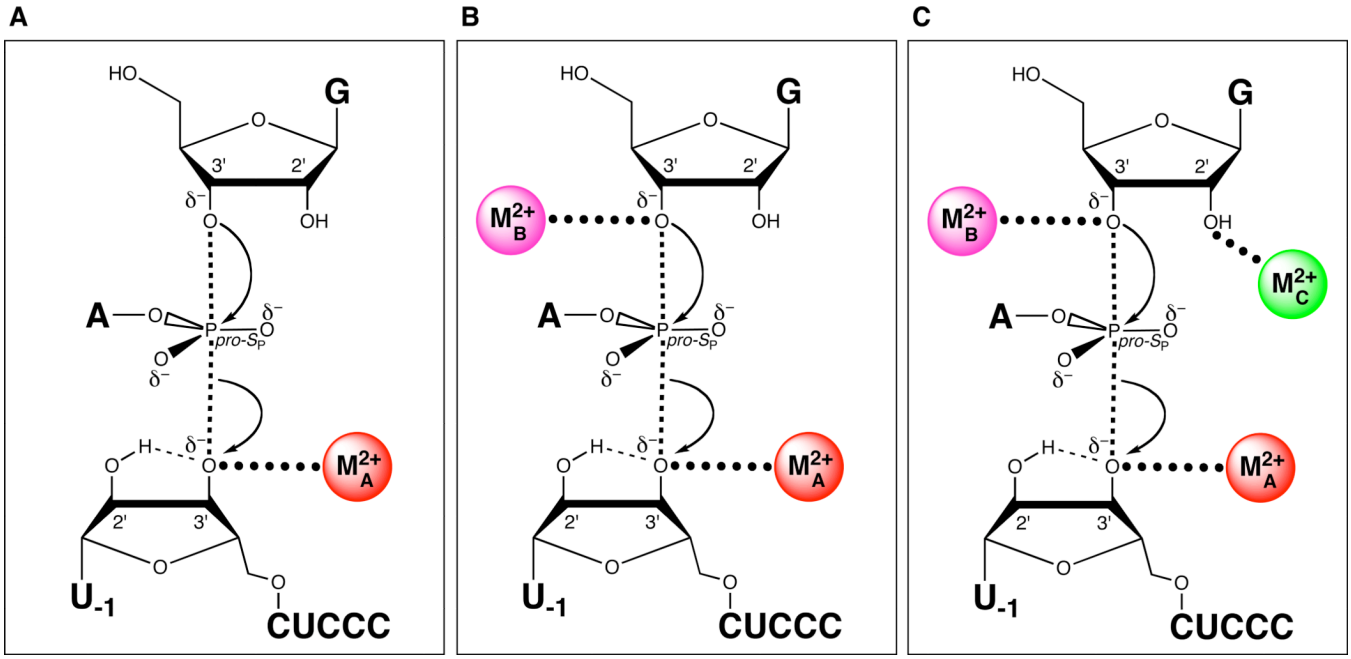

Figure 8.

Sequential discovery of three different catalytic metal ion-ligand interactions in the transition state of the *Tetrahymena* group I ribozyme reaction. (A) M_A coordinates the 3' oxygen of the leaving group. (B) M_B coordinates the 3'-OH of the guanosine nucleophile. (C) M_C coordinates the 2'-OH of the guanosine nucleophile.

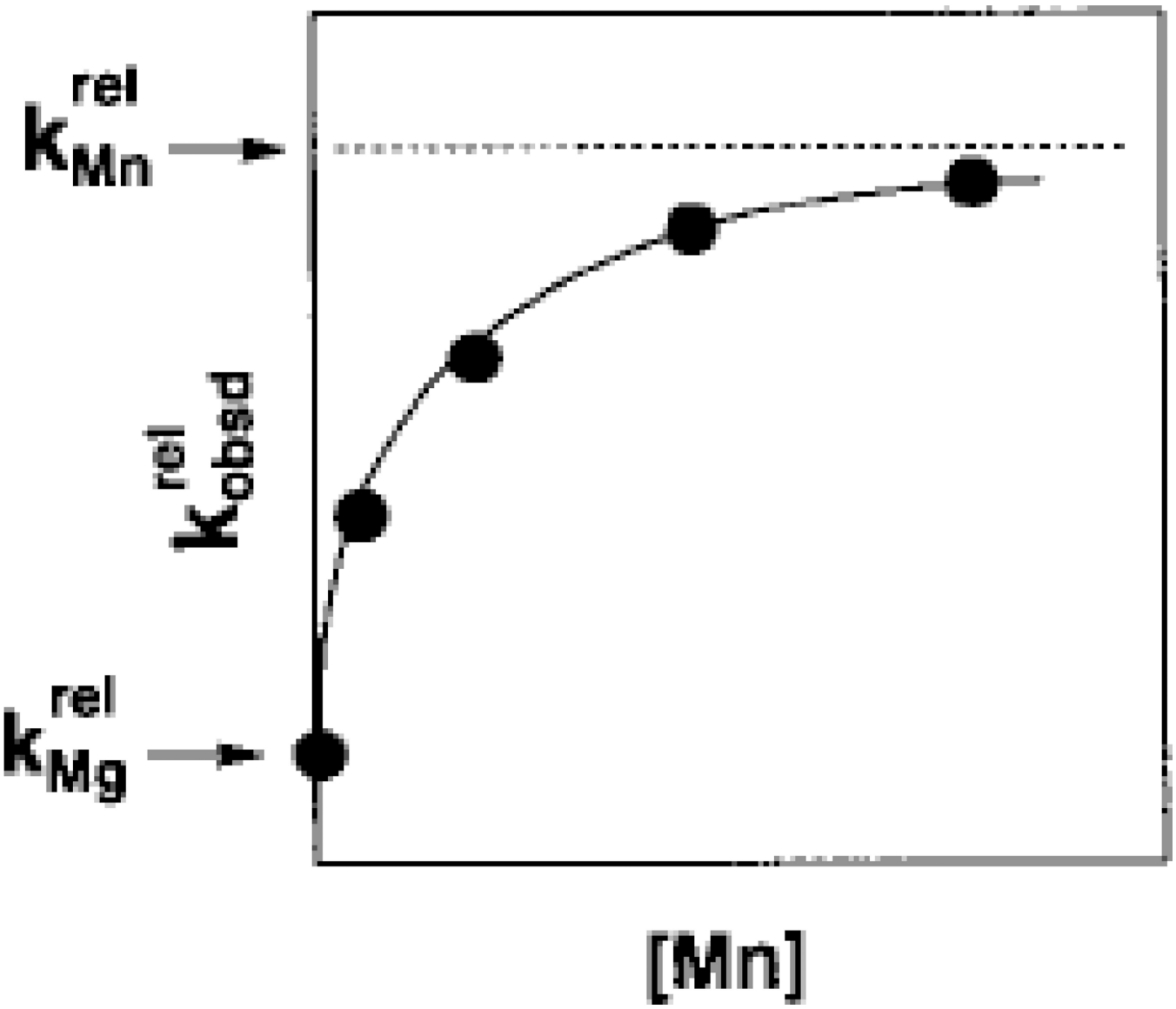

Figure 9.

Mn^{2+} concentration dependence of the reaction of $S_{3'S}$ relative to $S_{3'O}$ (k_{obs}^{rel}) for the reaction shown in Scheme 1. The Mn^{2+}-dependent acceleration of the reaction is associated with a specific affinity (K^{Mn}) of the rescuing Mn^{2+} ion for the free ribozyme. This affinity is a thermodynamic fingerprint for Mn^{2+} rescue of the 3' sulfur modification. [Taken from (121).]

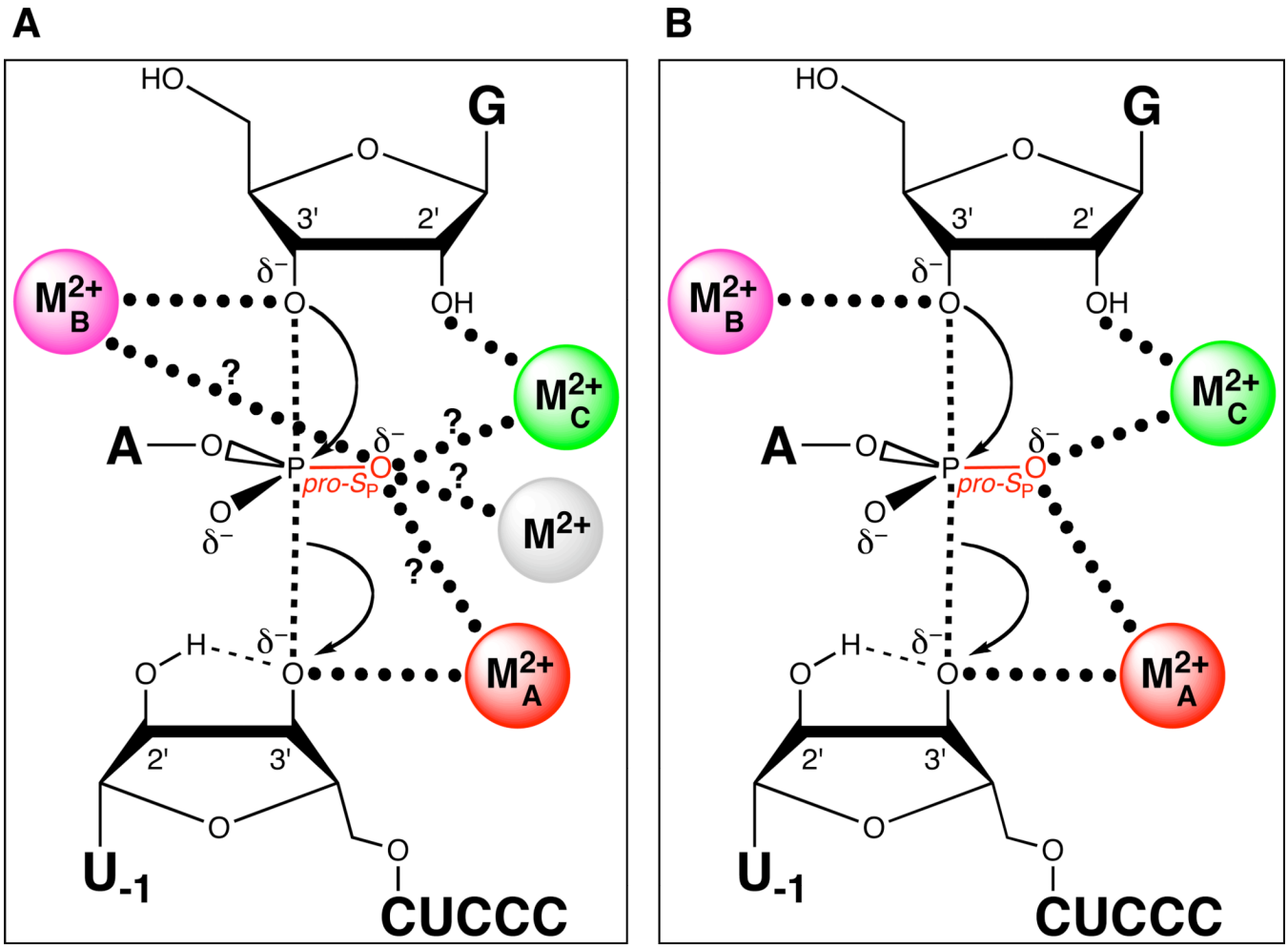

Figure 10.

Both M_A and M_C coordinate the *pro-*S_P nonbridging oxygen of the scissile phosphate. (A) Model showing potential metal ion-ligand interactions involving the *pro-*S_P nonbridging oxygen (question marks). The grey sphere denotes a fourth divalent metal ion, a possibility not excluded from the results in (123). (B) Revised transition state model based on (124). Three metal ions are present in the active site, with metals A and C coordinating the *pro-*S_P nonbridging oxygen of the scissile phosphate.

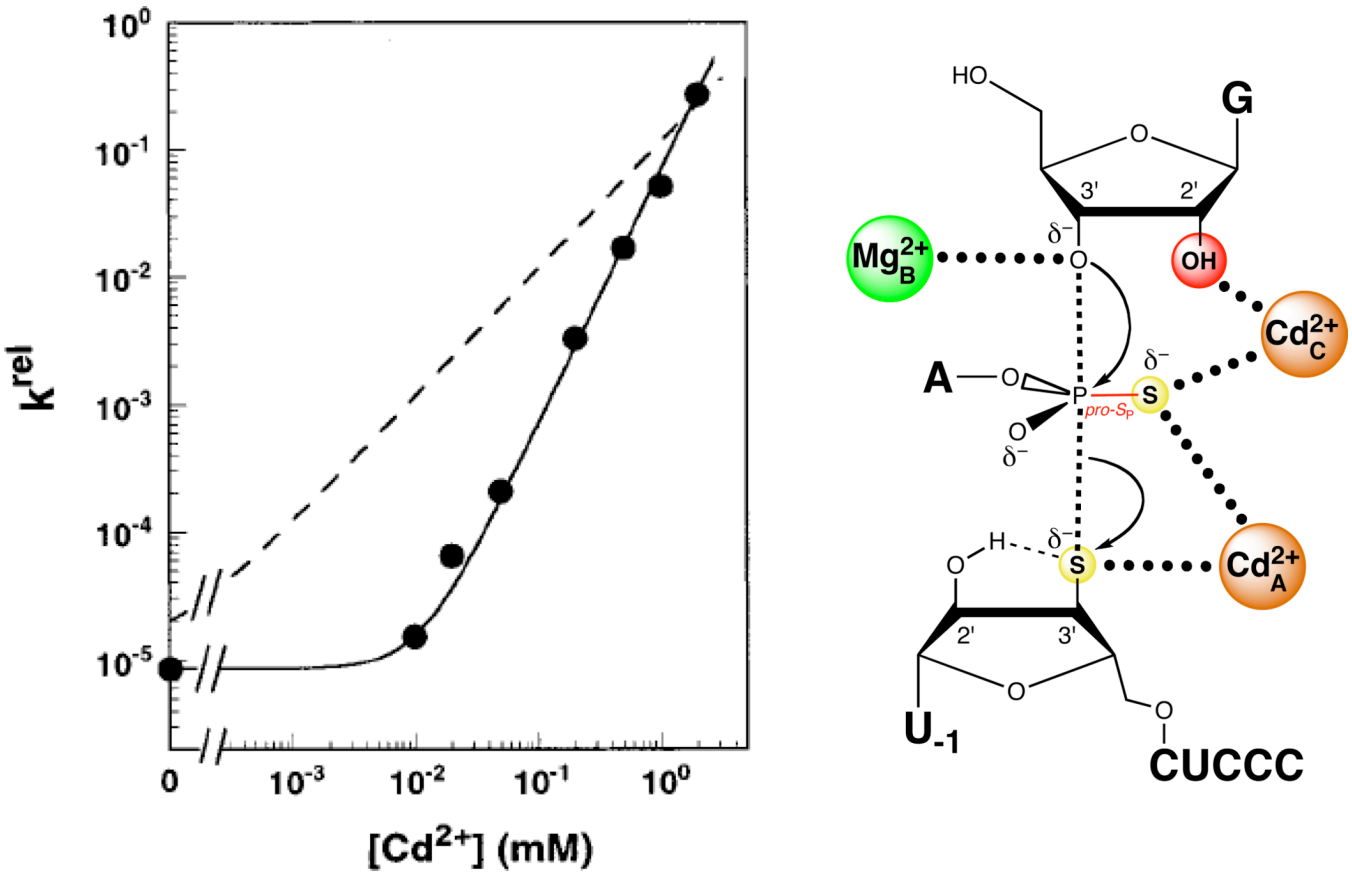

Figure 11.

Two Cd^{2+} ions at sites A and C rescue the reaction of $S_{3'S,P\text{-}S}$ by the *Tetrahymena* ribozyme. The plot at left shows the Cd^{2+} concentration dependence of k^{rel}, the reaction rate constant for $S_{3'S,P\text{-}S}$ relative to that of an all-oxygen substrate. The solid line fits the data according to a model in which two Cd^{2+} ions rescue the reaction, while the dashed line fits the data according to a model in which a single Cd^{2+} ion mediates rescue. [Data taken from (124).]

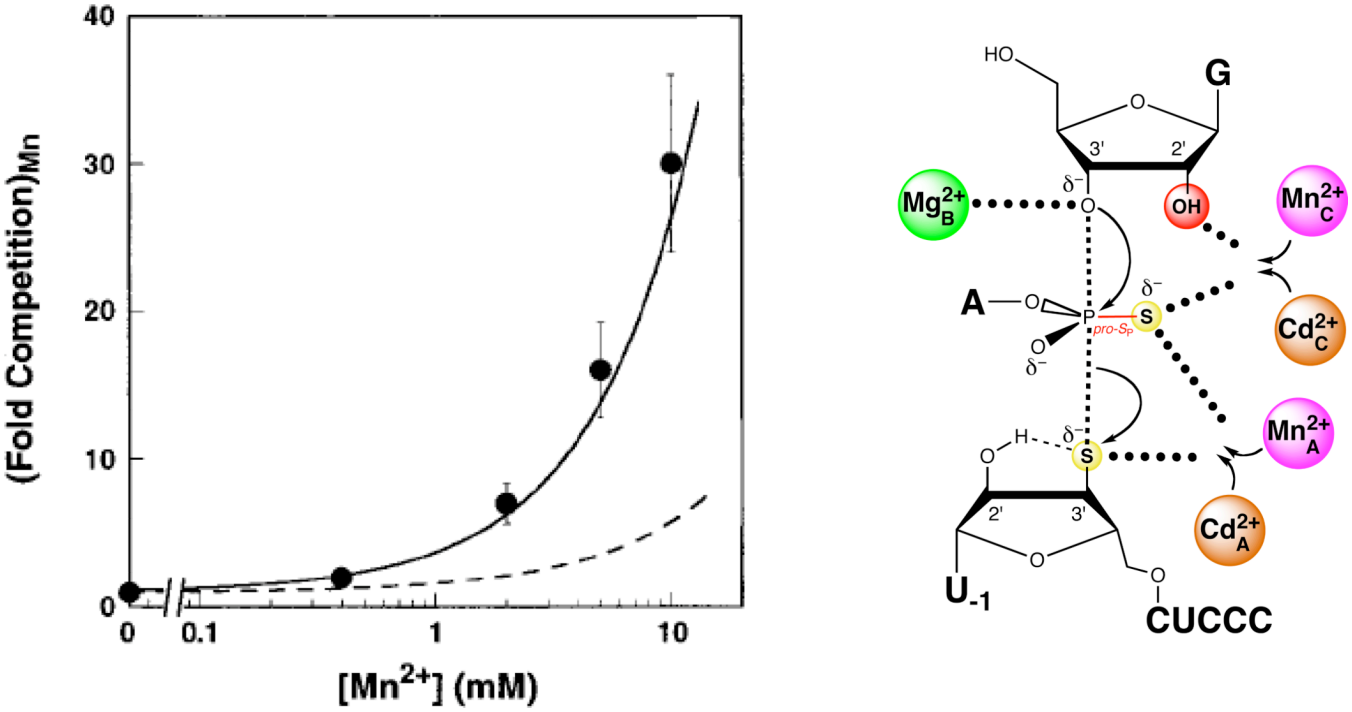

Figure 12.

Mn^{2+} ions compete with Cd^{2+} ions for sites A and C during rescue of the $S_{3'S,P\text{-}S}$ reaction. In the plot at left, the data are represented as filled spheres. The solid line shows the degree of competition expected from Mn^{2+} ions competing at sites A and C, while the dashed line shows the corresponding model for Mn^{2+} competition at sites A and B. [Data taken from (124).]

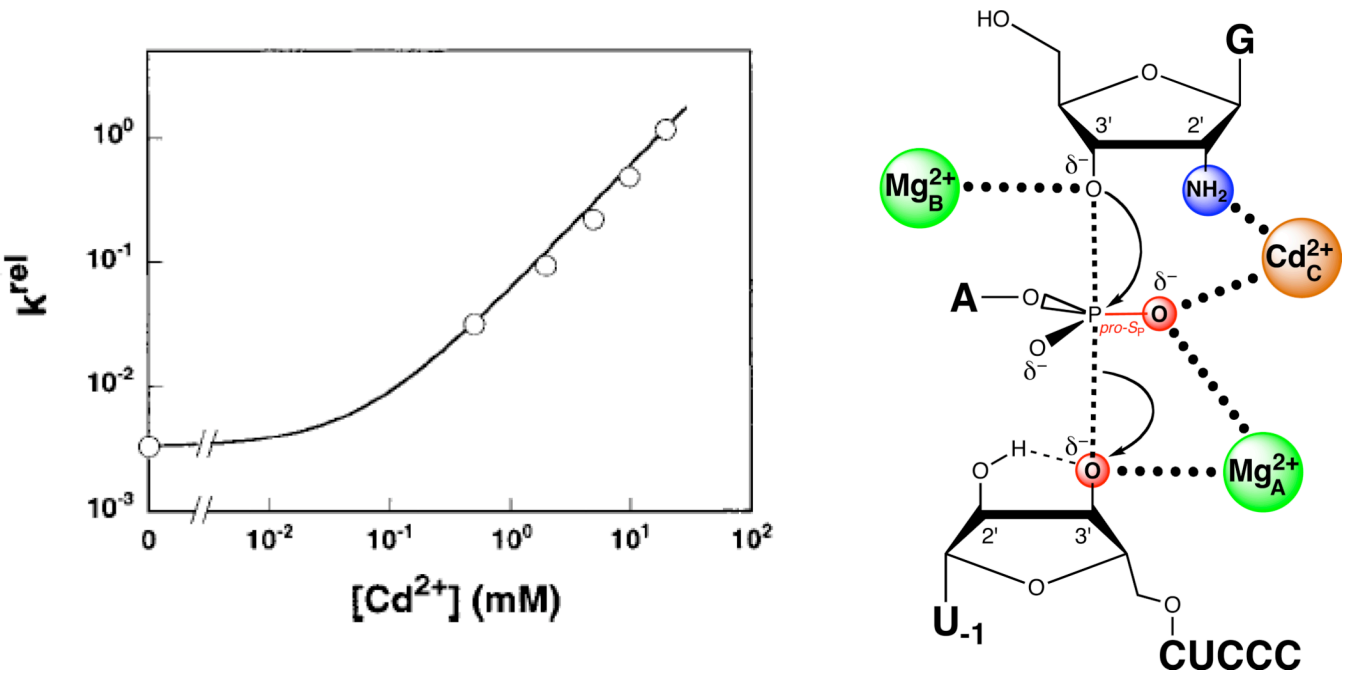

Figure 13.

A single Cd^{2+} ion rescues the reaction in which $G_{2'NH_2}$ replaces guanosine. The plot at left shows the Cd^{2+} dependence of the rate constant for the reaction involving $G_{2'NH_2}$relative to guanosine for the all-oxygen substrate. The data are fit to a model in which a single Cd^{2+} ion rescues the reaction. [Data taken from (124).]

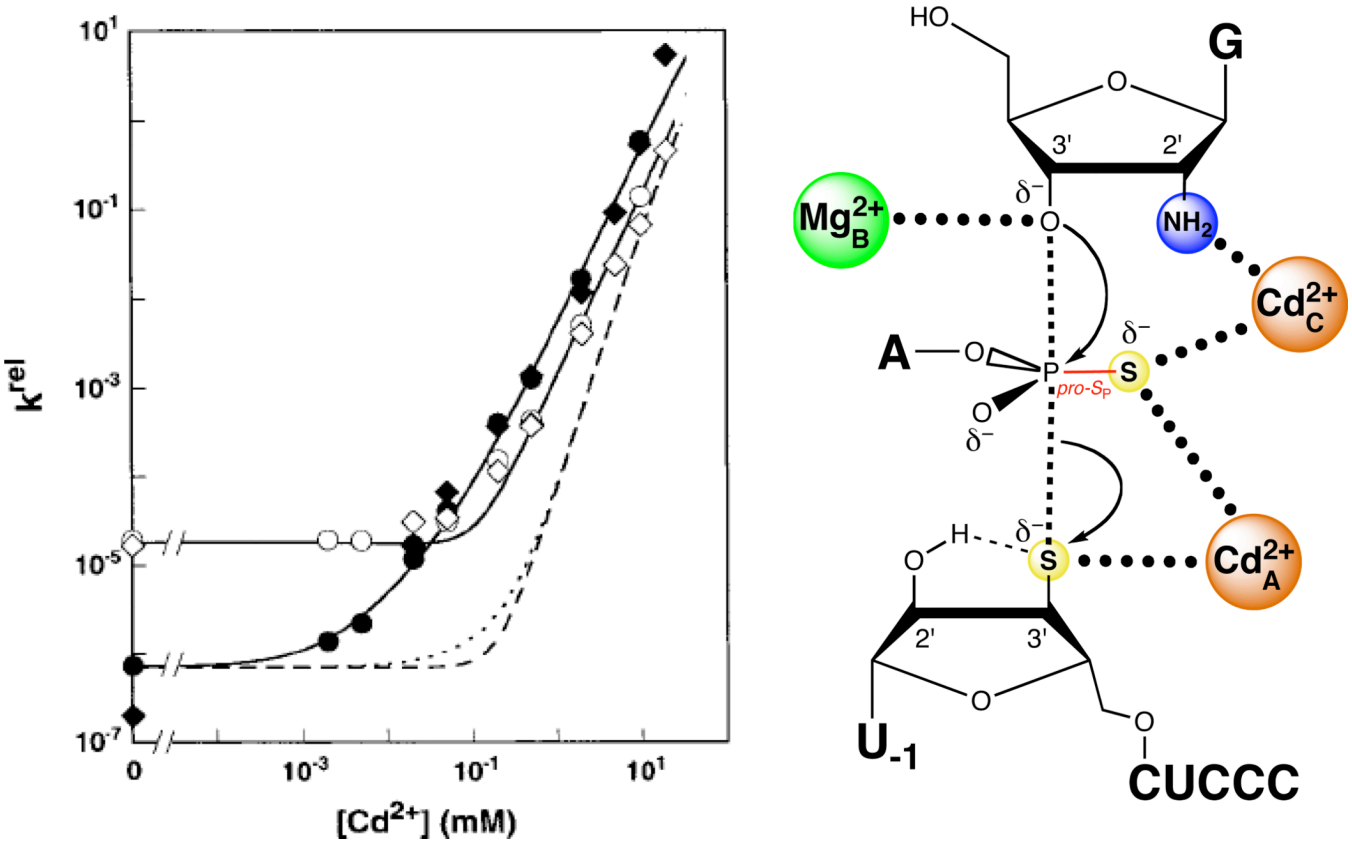

Figure 14.

Two Cd^{2+} ions rescue the reaction of $S_{3'S,P\text{-}S}$ with $G_{2'NH_2}$. In the plot at left, the closed symbols denote two independent determinations of the Cd^{2+} dependence of the reaction of $S_{3'S,P\text{-}S}$ with $G_{2'NH_2}$, relative to that of the all-oxygen substrate with guanosine. The open symbols denote two independent determinations of k^{rel} for the reaction of $S_{3'S,P\text{-}S}$ with guanosine, compared to that of the all-oxygen substrate with guanosine. The solid lines are fits of the data to a model in which two Cd^{2+} ions rescue the reaction, while the dashed lines are fits in which three Cd^{2+} ions rescue the reaction. [Data taken from (124).]

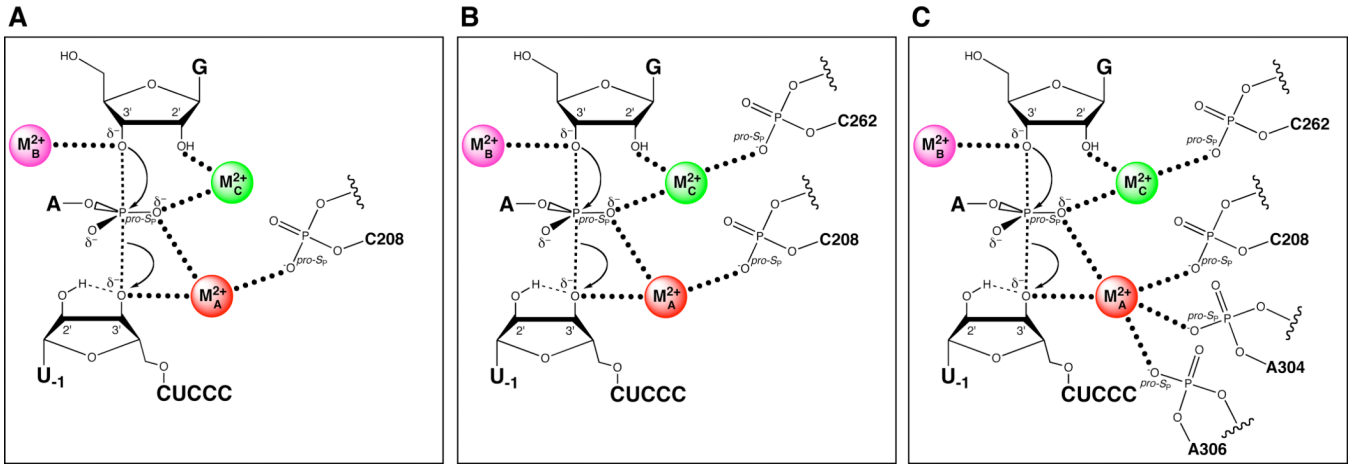

Figure 15.

Sequential discovery of ligands within the *Tetrahymena* ribozyme that position the catalytic metal ions. (A) The *pro-S*$_P$ nonbridging oxygen of C208 coordinates M_A. (B) The *pro-S*$_P$ nonbridging oxygen of C262 coordinates M_C. (C) Additional ligands for M_A include The *pro-S*$_P$ nonbridging oxygens of A304 and A306.

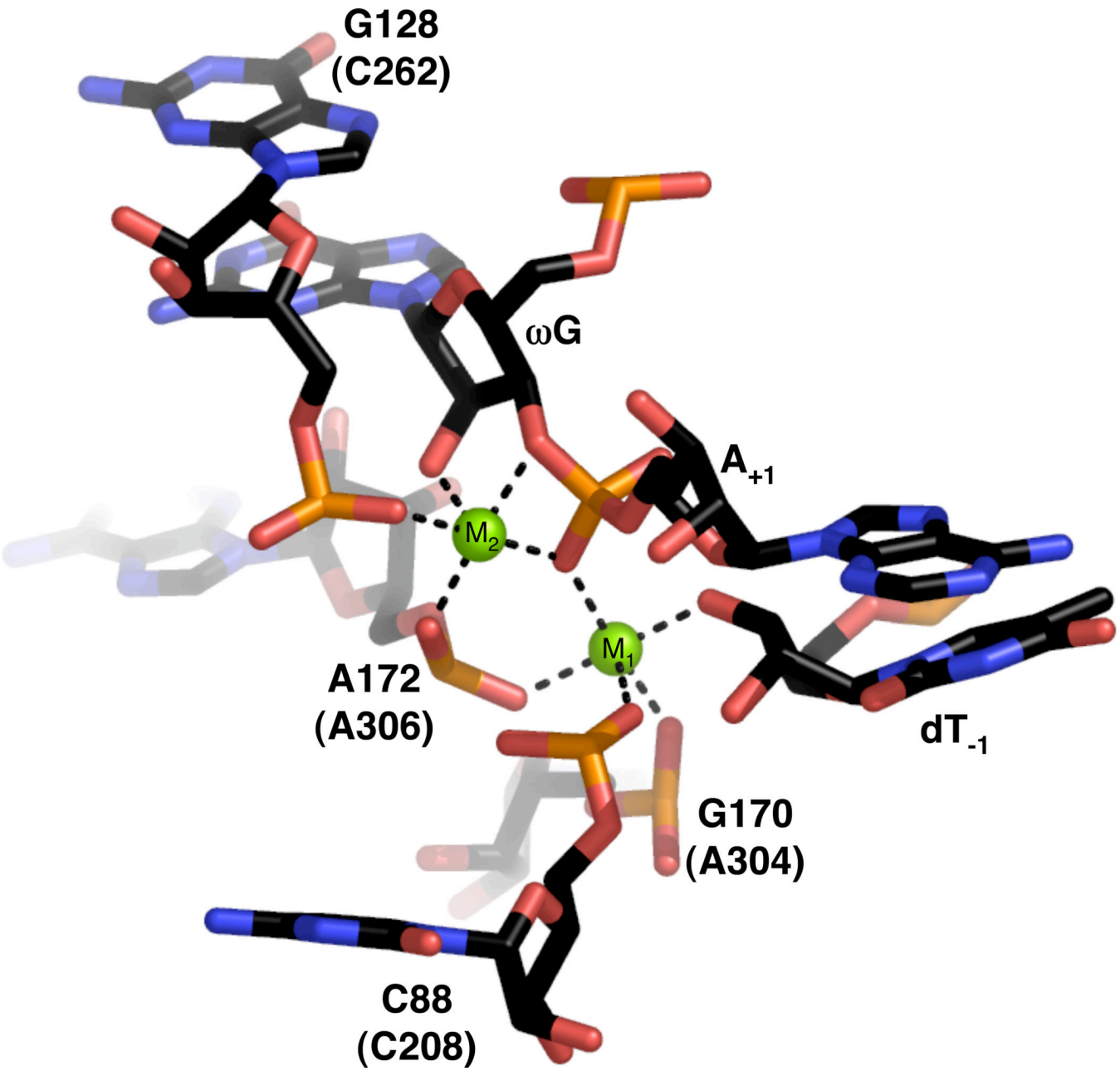

Figure 16.
View of the active site of the *Azoarcus* group I ribozyme (PDB file 1ZZN). Nucleotide numbers in parentheses refer to homologous positions within the *Tetrahymena* ribozyme. Mg^{2+} ions are represented as green spheres. Black lines denote putative inner sphere interactions between ribozyme ligands and the metal ions.

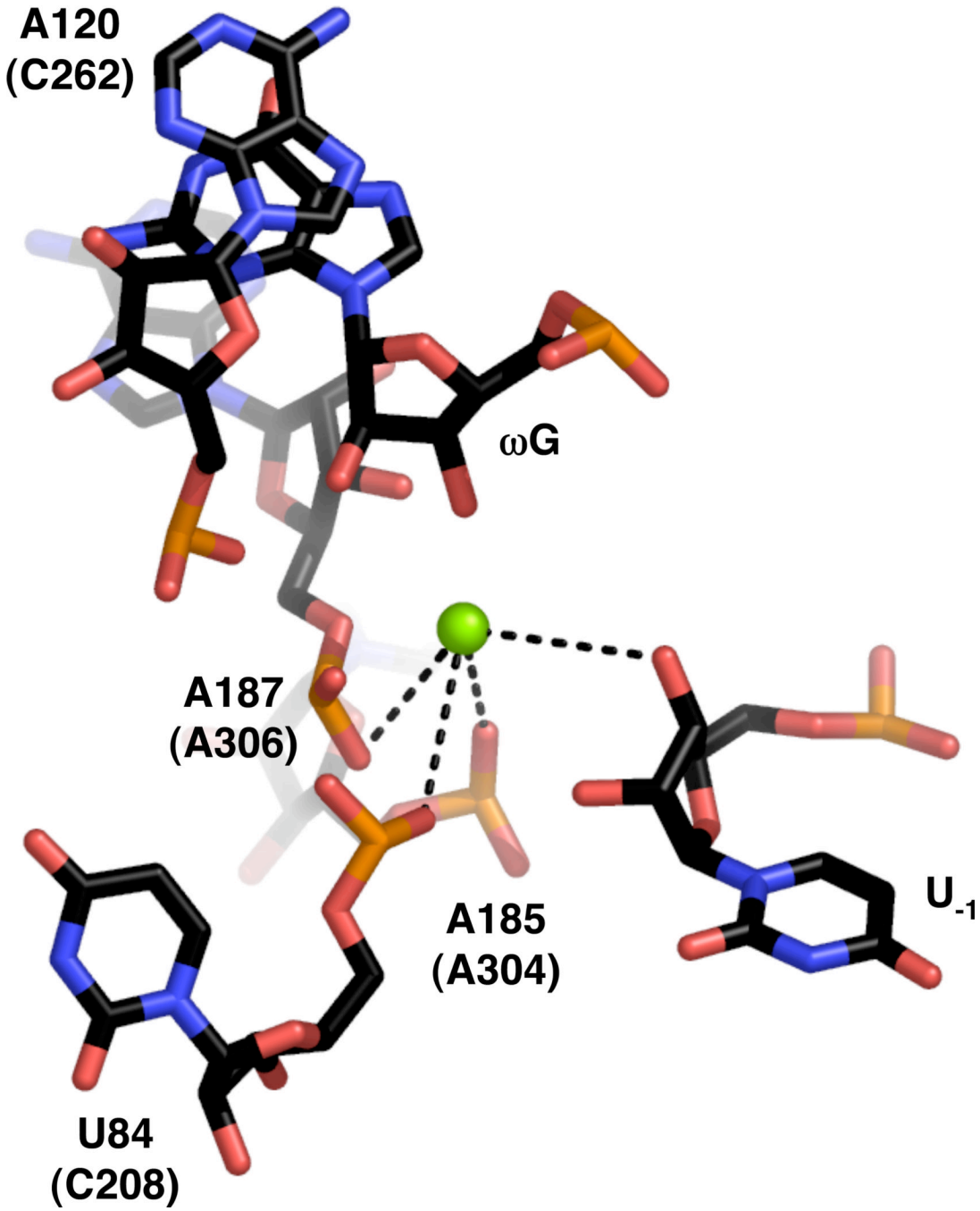

Figure 17.
View of the active site of the group I ribozyme derived from bacteriophage *Twort* (PDB file 1Y0Q). Numbering and colors are as in Figure 16.

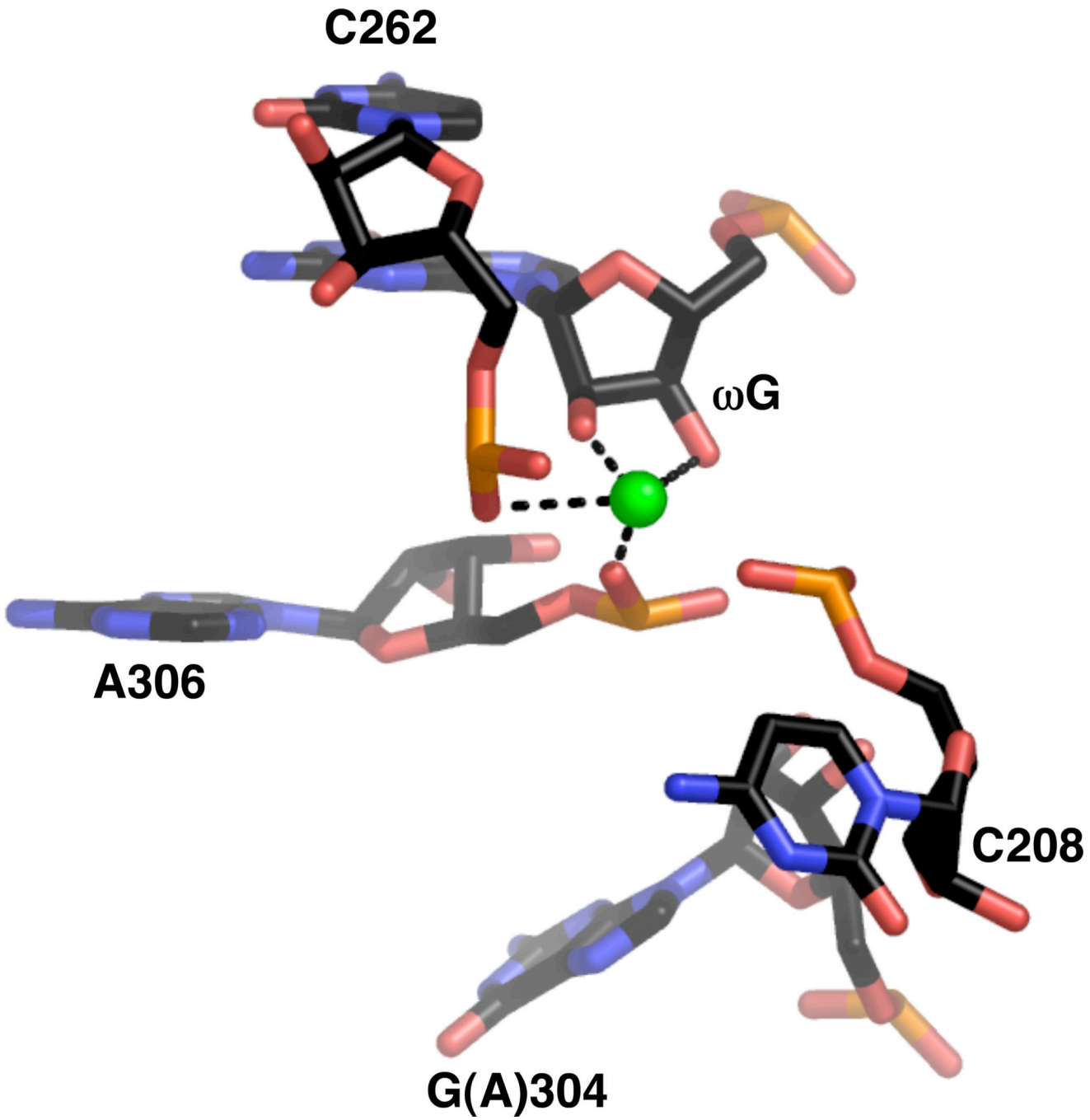

Figure 18.
Active site metal ion within the crystal structure of the *Tetrahymena* ribozyme (PDB file 1X8W). The guanosine at position 304 is one of several mutations introduced based on experiments that selected for thermostable variants of the ribozyme.

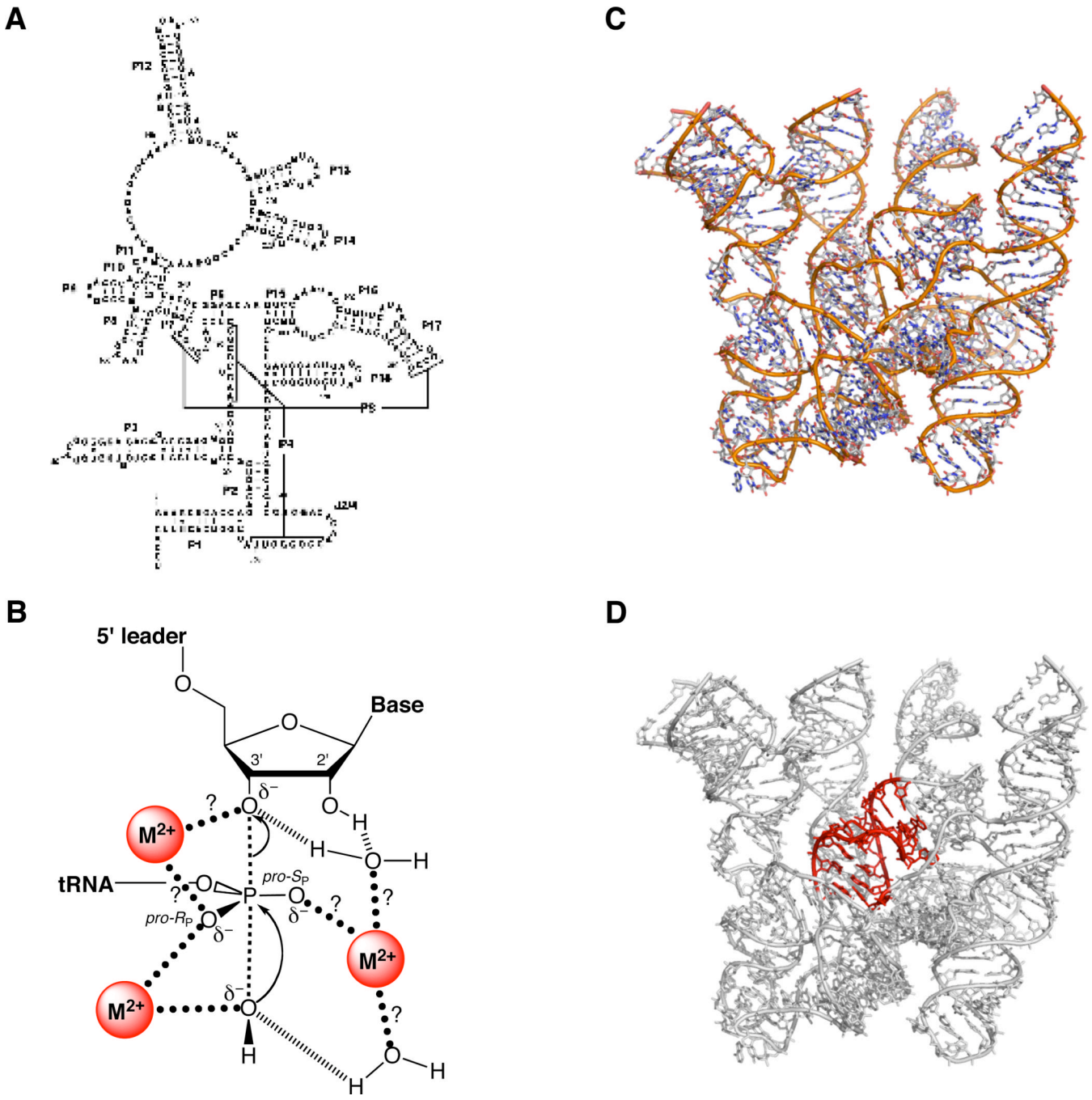

Figure 19.
The RNA component of RNase P. (A) Secondary structure of *E. coli* P RNA. (B) Transition state model for the reaction catalyzed by RNase P. Question marks denote putative metal ion-ligand interactions awaiting experimental verification. [Adapted from (175), with permission.] (C) Crystal structure of the P RNA from *B. stearothermophilus* at 3.3 Å (PDB file 2A64). (D) Location (in red) of the P4 helix within the *B. stearothermophilus* P RNA.

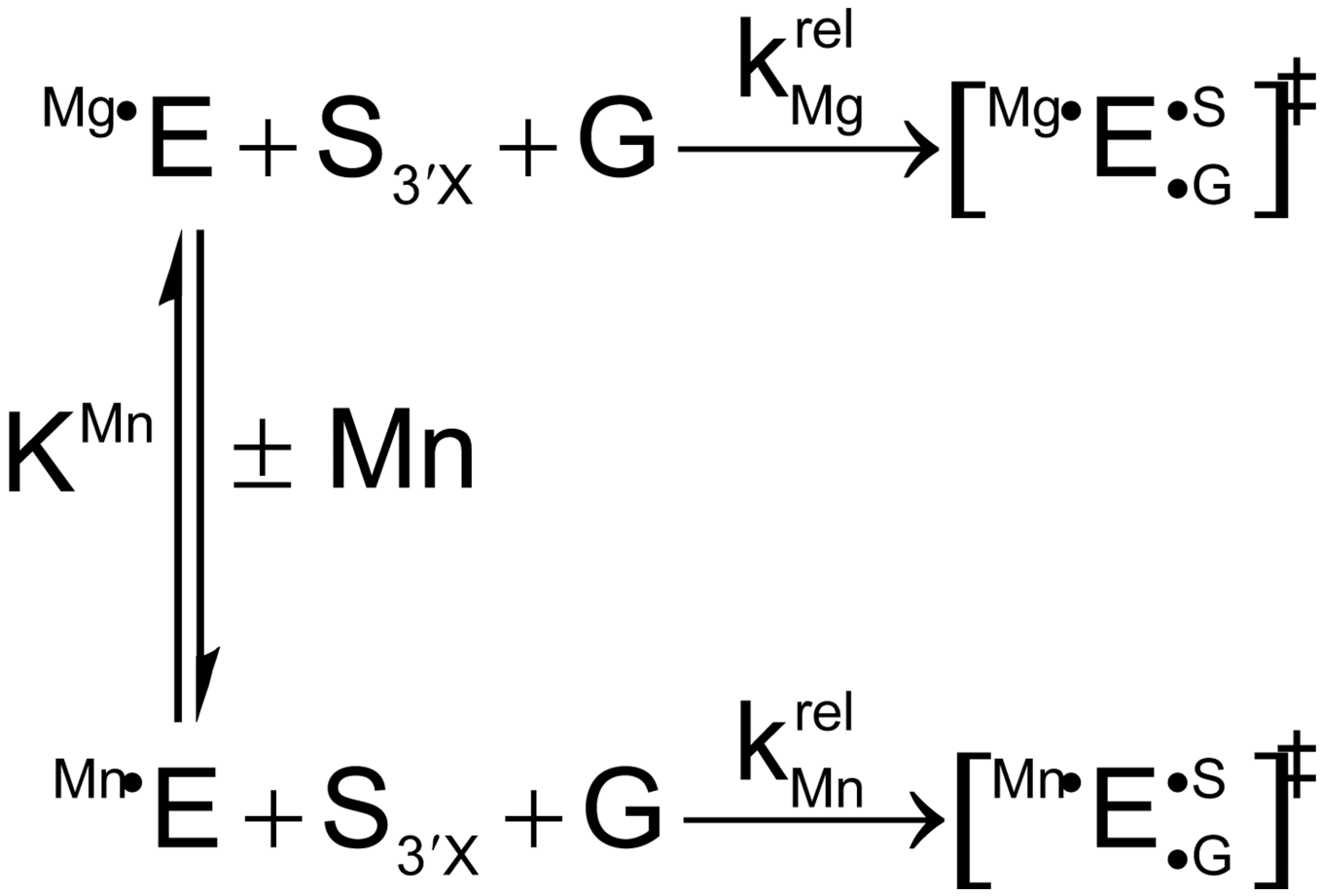

Scheme 1.